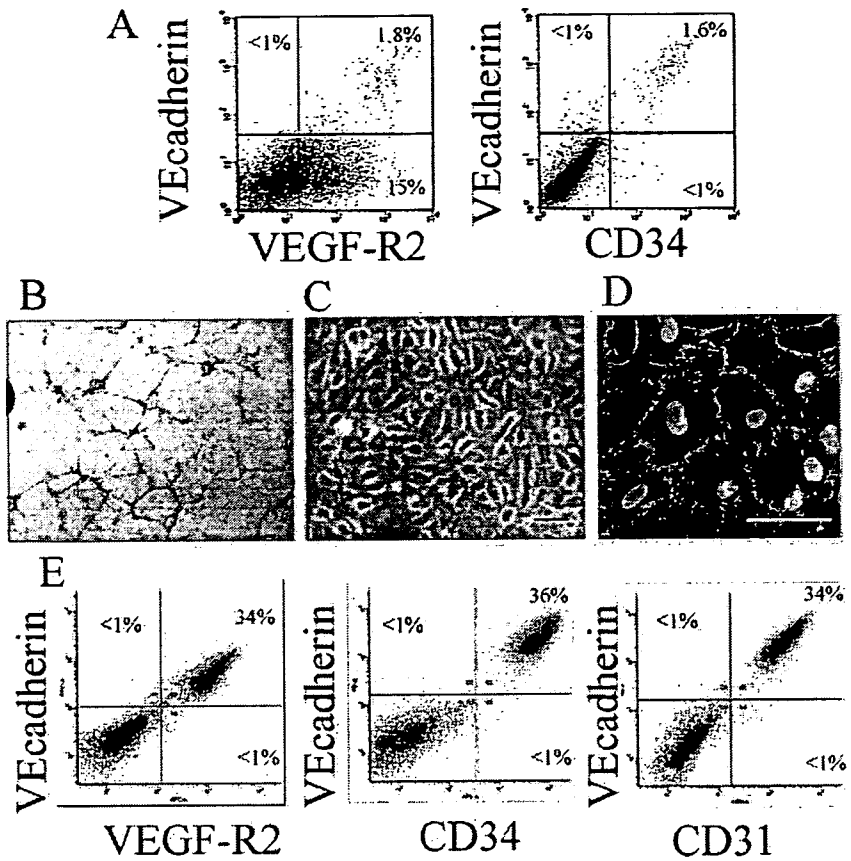

Figure 3. Isolation and expansion of vascular eECs. A, Flow-cytometric analysis of human ES cell–derived cells on an OP9 feeder layer on day 10. B, Network formation of human ES cell–derived VE-cadherin$^+$ cells (eECs) after 24-hour culture on Matrigel. C, Phase-contrast microscopic analysis of recultured VE-cadherin$^+$ cells on a collagen IV–coated dish. D, Immunostaining of recultured VE-cadherin$^+$ cells; red, CD31; green, nuclear staining (SYBR-Green I). E, Flow-cytometric analysis of the cells at the sixth passage expanded from VE-cadherin$^+$ cells. Scale bar, 50 μm.

muscle actin expression (Figure 2E). In the absence of VEGF, VEGF-*R2*$^+$ TRA1-60$^-$ cells did not differentiate into ECs, but almost all of them differentiated into α-smooth muscle actin and calponin-positive cells, which can be categorized as MCs (Figure 2F and 2G). Because these VEGF-*R2*$^+$ TRA1-60$^-$ cells expressed PDGFRβ, PDGF-BB with 0.5% FCS induced MC induction in a similar manner (Figure 2H). We, therefore, concluded that these VEGF-*R2*$^+$ TRA1-60$^-$ cells could be categorized as human VPCs that can differentiate into both ECs and MCs. Next we examined whether VEGF-*R2*$^+$ TRA1-60$^+$ cells after 8 days of differentiation is immature or not. Before differentiation, VEGF-*R2*$^+$ TRA1-60$^+$ cells were positive for flt1, AC133, and c-Kit and negative for CXCR4, PDGFRα, PDGFRβ, CD34, and VE-cadherin. However, after 8 days of differentiation, c-Kit expression decreased, and PDGFRα-positive and/or β-positive cells appeared in VEGF-*R2*$^+$ TRA1-60$^+$ cells (data not shown). Thus, VEGF-*R2*$^+$ TRA1-60$^+$ cells after 8 days of differentiation were not equivalent to the immature ES cells on day 0.

Isolation and Expansion of Vascular eECs

Next, we focused our attention on VE-cadherin$^+$ ECs that were more differentiated than the VPC. On 10 days of differentiation of HES3 on an OP9 feeder layer, VEGF-*R2*$^+$ and VE-cadherin$^+$ cells emerged and accounted for $\approx$1% to 2% of all the cells (Figure 3A). This VE-cadherin–positive cell population was almost identical to the CD34$^+$ population (Figure 3A). We sorted these VE-cadherin$^+$ cells, and, because these cells were also VEGF-*R2*$^+$ and CD34$^+$ (Figure 3A), we used the term "eEC" for these EC in the early differentiation stage. These cells formed a network-like structure on Matrigel in vitro (Figure 3B), showed a cobblestone appearance when they became confluent (Figure 3C), and immunofluorescence staining with CD31 showed a characteristic marginal staining pattern (Figure 3D). These eECs were negative for monocyte makers CD45, CD11b, and CD14 (data not shown) and could be successfully propagated by a factor of $\approx 1.2\times10^2$ (from 2×10^5 cells to 2.4×10^7 cells) after 6 passages on collagen IV–coated dishes. They were cultured with a cell density of 1.5×10^4 cells/cm^2 with VEGF because they did not expand when they were more sparsely plated or cultured without VEGF. Flow-cytometric analysis showed that VE-cadherin$^+$ cells were reduced to $\approx$35% of the total number of cells after 6 passages (Figure 3E), but they were still VEGF-*R2*$^+$, CD34$^+$, and CD31$^+$ at the sixth passage, indicating that the cell differentiation stage had been maintained (Figure 3E). In another series of experiments, we sorted these VE-cadherin$^+$ cells on day 10 and replated them on an OP9 feeder layer or nonfeeder collagen IV–coated dishes for 1 additional week. The VE-cadherin$^+$ cells in these 2 culture groups were then resorted and plated on nonfeeder collagen IV–coated dishes for reculturing. After an additional 3 weeks of reculturing, VE-cadherin expression was examined. The cells that were cultured for 1 additional week on OP9 were 90% positive for VE-cadherin, but the cells kept on nonfeeder dishes were only 44% positive. This suggests that VE-cadherin$^+$ eECs still retain the potential to differentiate

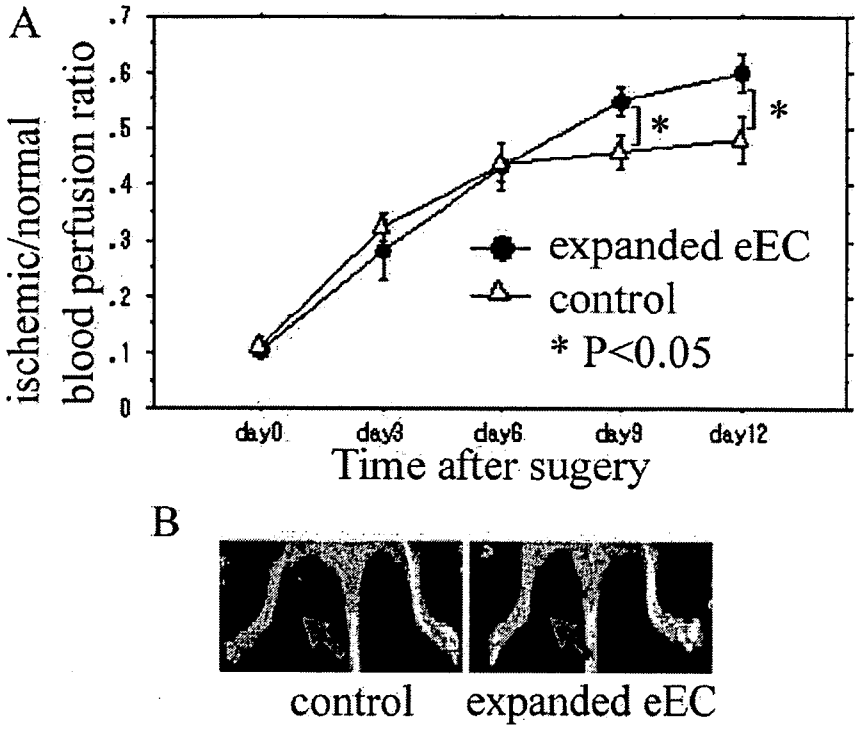

Figure 4. Transplantation of human ES cell–derived vascular cells to the hindlimb ischemia model of immunodeficient mice. A, Quantitative analysis of the hindlimb blood flow by means of calculating the ischemic/normal limb perfusion ratios in mice with ischemic hindlimb. *$P<0.05$. On days 9 and 12, the blood flow in the ischemic limb of the expanded eEC-injected mice (n=8) had increased significantly compared with that of control mice (n=8). B, Representative laser Doppler perfusion images on day 12.

into other cell types, but more differentiated VE-cadherin$^+$ ECs may lose this ability.

Transplantation of Human ES Cell-Derived Vascular Cells to the Hindlimb Ischemia Model of Immunodeficient Mice

As the next step, we investigated whether human ES cell–derived vascular cells can be used for vascular regeneration in cell transplantation in the hindlimb ischemia model. KSN nude mice received an intra-arterial injection of cells in PBS or PBS only into the right femoral artery, followed by right femoral artery ligation and removal to create hindlimb ischemia. VEGF-$R2^+$ TRA1-60^- cells, identified as VPCs, were transplanted, but laser Doppler perfusion image analysis on day 14 showed no significant difference in recovery of the blood flow (expressed as the ischemic/normal limb blood perfusion ratio) between the cell-transplanted mice (0.496±0.29; n=10) and the control PBS-injected mice (0.433±0.42; n=14). Next, we used the eECs expanded at passages 4 to 6. As shown in Figure 4A and 4B, the hindlimb blood flows had significantly improved in the cell-injected group 9 and 12 days after injection. For histological analysis, transplanted cells had been labeled with CM-DiI before cell transplantation, and biotin-conjugated isolectin B_4 was intravenously injected to stain ECs before sacrifice on day 14. Although some of the transplanted cells were incorporated as isolectin B4$^+$ vascular ECs in the large vessels (Figure 5A), most of the transplanted cells were incorporated as small capillaries (Figure 5B). To quantify the capillary density, sections of the ischemic hindlimbs were stained with anti-mouse and human-specific CD31 antibodies (Figure 5C and 5D). Human CD31$^+$ capillaries were detected in the expanded eEC-transplanted mice. The mouse and/or human CD31$^+$ total capillary number and area significantly increased in the expanded eEC-transplanted group compared with the control PBS-injected group, whereas there was tendency but no significant difference in the mouse CD31$^+$ host capillary number and area (Figure 5E and 5F). On the other hand, there was no significant difference in the capillary length (Figure 5G). Because we cut our sections at right angles with muscle fibers and femoral artery, it might be difficult to estimate the capillary density by vessel length.

Next we performed our transplantation experiments with the same procedure using BALB/c Slc nude mice, in which hindlimb ischemia is more severe than in KSN/Slc nude mice. PBS, VPCs, eECs or human adult aortic ECs were transplanted, and the ischemic hindlimbs were observed on day 14. In the PBS-injected mice, the ischemic hindlimb was autoamputated in 3 of 7 mice, and mild necrosis was observed in 1 of 7. In the VPC-transplanted mice, 3 of 7 were autoamputated and mild necrosis was seen in 2 of 7. In the eEC-transplanted mice, the ischemic hindlimb was not autoamputated, and only mild necrosis was observed in 2 of 8. In the human adult aortic EC-transplanted mice, 4 of 7 were auto-amputated, and mild necrosis was seen in 1 of 7. Furthermore, sections of the ischemic hindlimb in mice without autoamputation were stained with anti-mouse and human-specific CD31 antibodies. Human CD31$^+$ capillaries were most abundant in the eEC-transplanted mice, although some human CD31$^+$ cells were detected in the VPC or human adult aortic EC-transplanted mice (please see http://atvb.ahajournals.org).

Exclusion of Possible Teratoma Formation by the Expanded eEC

Further experiments were conducted to detect possible teratoma formation by eEC. We conducted long-term follow-ups

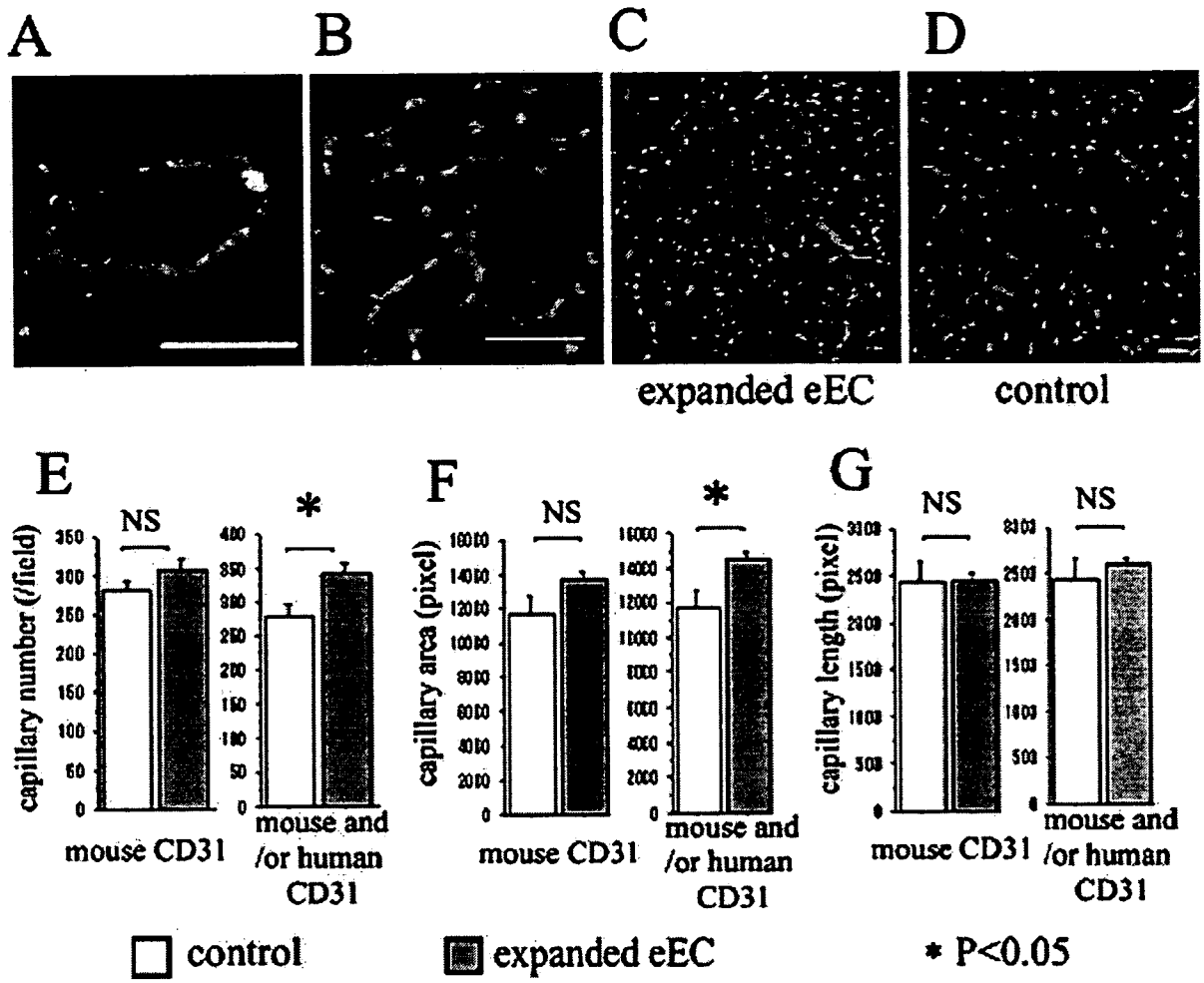

Figure 5. A and B, Histological analysis of vascular regeneration by the intra-arterially injected expanded eEC; green, isolectin B_4^+ endothelial cells; red, CM-DiI$^+$ transplanted cells (representative photographs). C and D, Fluorescent photographs of ischemic hindlimb for capillary density analysis; green, mouse CD31$^+$ capillaries; red, human CD31$^+$ capillaries (representative photographs). E through G, Quantitative analysis of the mouse and human endothelial cell marker–positive capillary densities in the ischemic hindlimb. E, capillary numbers. F, capillary areas. G, capillary lengths. Scale bars, 50 μm.

by transplanting expanded eECs or undifferentiated human ES cells into 3 mice each and following them for 5 months. We transplanted 5×10^5 cells under the dorsal back skin of SCID mice, which are commonly used for teratoma formation for human ES cells. Large tumors had formed after 3 to 5 months in 2 of the 3 mice in the human ES cell–transplanted group, but none had formed in any of the 3 mice in the expanded eEC-transplanted group. In immunohistological analysis, HLA-ABC$^+$ tumors were not observed in the subcutaneous region of eEC transplanted mice, although only a few HLA-ABC$^+$ human cells were remaining (data not shown).

Expression of Angiogenic Factors in Human ES Cell–Derived Vascular Cells

In addition, we investigated whether VPC or eEC produced major angiogenic factors such as VEGF, bFGF, human growth factor, and PDGF-BB. RT-PCR analysis detected mRNA expressions of VEGF, bFGF, and human growth factor in VPCs and PDGF-B and bFGF in eECs (please see http://atvb.ahajournals.org). We measured the protein concentration of these angiogenic factors in culture media by ELISA; however, the concentration of VEGF, human growth factor, and PDGF-BB did not reached the detectable level, and the concentration of bFGF was <30 pg/mL.

Discussion

In this study, we were able to clarify the differentiation process from human ES cells to mature vascular cell components. In adults, VEGF and PDGF receptors are expressed on EC and MC, respectively, and VEGF and PDGF stimulate the growth of the respective cell types. In this study, human ES cell–derived VPCs expressed both VEGF and PDGF receptors. In addition, stimulation with VEGF and PDGF-BB induced 2 differentiation pathways for EC and MC in this cell population. In mouse embryos, VEGF-*R*2 and PDGFRα were reported to be expressed in the mesoderm.[11] In whole-mount immunohistochemistry of mouse embryos (E7.5 to 8), VEGF-*R*2 was expressed predominantly in the extraembryonic and proximal-lateral mesoderm. PDGFRα was detected mainly in the paraxial embryonic mesoderm. Both VEGF-*R*2 and PDGFRα were

detected in the anterior paraxial mesoderm. It was also reported that vascular endothelial precursors were identified from the cephalic mesoderm of the avian embryo labeled using an antibody against Quek1 (avian homolog of VEGF-*R*2).[12] Our result that VEGF-*R*2$^+$ PDGFR$^+$ VPCs can differentiate into vascular cells may agree with their reports. In our transplantation examination, some human CD31$^+$ ECs were observed in the ischemic hindlimb of VPC-transplanted mice. This suggests that some transplanted VPC (negative for CD31) differentiated into CD31$^+$ ECs in vivo.

In addition, we investigated whether human ES cell–derived vascular cells can be used for vascular regeneration. Transplanted eECs were successfully incorporated into the host circulation and significantly accelerated improvement of local blood flow, whereas VPCs did not. We reported recently that VEGF-*R*2$^+$ cells derived from mouse ES cells could differentiate into not only vascular cells but also cardiomyocytes.[13] Thus, VPCs may be too immature to be used directly as the source for vascular regeneration. It has also been reported that ischemia-induced neovascularization did not improve in mice receiving human mature ECs (eg, human microvascular ECs).[14] Their report is compatible with our result that human adult aortic EC transplantation had no effect for the prevention of ischemic necrosis. The induction and isolation of the cells at the differentiation stage most appropriate for transplantation seem to be important. Judging from our results obtained from histological analysis and capillary density evaluation, at least some of the therapeutic effect of transplantation of expanded eECs could be attributed to vascular regeneration as a result of incorporation of the transplanted cells into the host vessels. Because RT-PCR analysis detected mRNA expression of PDGF-B not in VPCs but in eECs, PDGF-BB secretion might affect the effect of eEC transplantation, although PDGF-BB did not reached the detectable level in culture media. In adults, endothelial progenitor cells (EPCs) reportedly participate in postnatal angiogenesis,[15] whereas other reports suggest that EPCs contribute to neovascularization in tissue ischemia.[14] However, the expansion of EPCs in sufficient quantities to improve blood flow in large animals has not yet been achieved. In addition, some recent reports suggest that adult bone marrow–derived cells, such as EPCs, do not transdifferentiate into ECs under physiological conditions.[16,17] Although the role of EPCs as a modifier of vascular growth awaits further investigation, our findings may help provide an alternative and novel supply of vascular cells for cell therapy as a contribution to vascular regenerative medicine.

Furthermore, the establishment of an in vitro differentiation system of human vascular cell components from human ES cells in this study should also make it possible to dissect out cellular mechanisms in human vascular development and diseased states for which the knockout animal research approach is not practical. Trials on gene expression profiling using our in vitro differentiation system of human vascular cells from human ES cells could assist in the search for novel gene products to develop new therapeutic approaches for vascular regeneration.

Acknowledgments

The human ES cells (HES-3) were contributed by ES Cell International Pte Ltd, Singapore. The anti-human VEGF-*R*2 antibody (KM1668) was a generous gift from M. Shibuya, MD, PhD, Department of Cancer Biology, Institute of Medical Science, University of Tokyo.

Sources of Funding

This work was supported by Grants-in-Aid for Scientific Research from the Ministry of Health, Labour and Welfare and the Ministry of Education, Culture, Sports, Science and Technology. This work was also supported by a grant from the Japan Smoking Foundation, a Japan Heart Foundation/Pfizer Japan Grant for Cardiovascular Disease Research, and a grant from the Study Group for Molecular Cardiology Research. This work was also supported by Fellowships of the Japan Society for the Promotion of Young Scientists and Establishment of International COE for Integration of Transplantation Therapy and Regenerative Medicine (COE program of the Ministry of Education, Culture, Sports, Science and Technology, Japan).

Disclosures

None.

References

1. Reubinoff BE, Pera MF, Fong CY, Trounson A, Bongso A. Embryonic stem cell lines from human blastocysts: somatic differentiation in vitro. *Nature Biotechnology*. 2000;18:399–404.
2. Yamashita J, Itoh H, Hirashima M, Ogawa M, Nishikawa S, Yurugi T, Naito M, Nakao K, Nishikawa S. Flk1-positive cells derived from embryonic stem cells serve as vascular progenitors. *Nature*. 2000;408:92–96.
3. Miyashita K, Itoh H, Sawada N, Fukunaga Y, Sone M, Yamahara K, Yurugi-Kobayashi T, Park K, Nakao K. Adrenomedullin provokes endothelial Akt activation and promotes vascular regeneration both in vitro and in vivo. *FEBS Lett*. 2003;544:86–92.
4. Yurugi-Kobayashi T, Itoh H, Schroeder T, Nakano A, Narazaki G, Kita F, Yanagi K, Hiraoka-Kanie M, Inoue E, Ara T, Nagasawa T, Just U, Nakao K, Nishikawa, SI. Yamashita, JK. Adrenomedullin/cyclic amp pathway induces notch activation and differentiation of arterial endothelial cells from vascular progenitors. *Arterioscler Thromb Vasc Biol*. 2006;26:1977–1984.
5. Kaufman DS, Hanson ET, Lewis RL, Auerbach R, and Thomson JA. Hematopoietic colony-forming cells derived from human embryonic stem cells. *Proc Natl Acad Sci U S A*. 2001;98:10716–10721.
6. Levenberg S, Golub JS, Amit M, Itskovitz-Eldor J, Langer R. Endothelial cells derived from human embryonic stem cells. *Proc Natl Acad Sci U S A*. 2002;99:4391–4396.
7. Fujioka T, Yasuchika K, Nakamura Y, Nakatsuji N, Suemori H. A simple and efficient cryopreservation method for primate embryonic stem cells. *Int J Dev Biol*. 2004;48:1149–1154.
8. Hirashima M, Kataoka H, Nishikawa S, Matsuyoshi N, Nishikawa S. Maturation of embryonic stem cells into endothelial cells in an in vitro model of vasculogenesis. *Blood*. 1999;93:1253–1263.
9. Yamahara K, Itoh H, Chun TH, Ogawa Y, Yamashita J, Sawada N, Fukunaga Y, Sone M, Yurugi-Kobayashi T, Miyashita K, Tsujimoto H, Kook H, Feil R, Garbers DL, Hofmann F, Nakao K. Significance and therapeutic potential of the natriuretic peptides/cGMP/cGMP-dependent protein kinase pathway in vascular regeneration. *Proc Natl Acad Sci U S A*. 2003;100:3404–3409.
10. Sone M, Itoh H, Yamashita J, Yurugi-Kobayashi T, Suzuki Y, Kondo Y, Nonoguchi A, Sawada N, Yamahara K, Miyashita K, Park K, Shibuya M, Nito S, Nishikawa S, Nakao K. Different differentiation kinetics of vascular progenitor cells in primate and mouse embryonic stem cells. *Circulation*. 2003;107:2085–2088.
11. Kataoka H, Takakura N, Nishikawa S, Tsuchida K, Kodama H, Kunisada T, Risau W, Kita T, Nishikawa SI. Expressions of PDGF receptor alpha, c-Kit and Flk1 genes clustering in mouse chromosome 5 define distinct

subsets of nascent mesodermal cells. *Dev Growth Differ.* 1997;39: 729–740.
12. Couly G, Coltey P, Eichmann A, Le Douarin NM. The angiogenic potentials of the cephalic mesoderm and the origin of brain and head blood vessels. *Mech Dev.* 1995;53:97–112.
13. Yamashita JK, Takano M, Hiraoka-Kanie M, Shimazu C, Peishi Y, Yanagi K, Nakano A, Inoue E, Kita F, Nishikawa S. Prospective identification of cardiac progenitors by a novel single cell-based cardiomyocyte induction. *FASEB J.* 2005;19:1534–1536.
14. Kalka C, Masuda H, Takahashi T, Kalka-Moll WM, Silver M, Kearney M, Li T, Isner JM, Asahara T. Transplantation of ex vivo expanded endothelial progenitor cells for therapeutic neovascularization. *Proc Natl Acad Sci U S A.* 2000;97:3422–3427.
15. Asahara T, Murohara T, Sullivan A, Silver M, van der Zee R, Li T, Witzenbichler B, Schatteman G, Isner JM. Isolation of putative progenitor endothelial cells for angiogenesis. *Science.* 1997;275: 964–967.
16. O'Neill TJ 4th, Wamhoff BR, Owens GK, Skalak TC. Mobilization of bone marrow-derived cells enhances the angiogenic response to hypoxia without transdifferentiation into endothelial cells. *Circ Res.* 2005;97: 1027–1035.
17. Zentilin L, Tafuro S, Zacchigna S, Arsic N, Pattarini L, Sinigaglia M, Giacca M. Bone marrow mononuclear cells are recruited to the sites of VEGF-induced neovascularization but are not incorporated into the newly formed vessels. *Blood.* 2006;107:3546–3554.

Am J Physiol Endocrinol Metab 293: E819–E825, 2007.
First published June 26, 2007; doi:10.1152/ajpendo.00681.2006.

Effects of ghrelin administration on decreased growth hormone status in obese animals

Hiroshi Iwakura,[1] Takashi Akamizu,[1] Hiroyuki Ariyasu,[1] Taiga Irako,[1] Kiminori Hosoda,[2] Kazuwa Nakao,[2] and Kenji Kangawa[1,3]

[1]*Ghrelin Research Project, Translational Research Center, Kyoto University Hospital;* [2]*Department of Medicine and Clinical Science, Endocrinology and Metabolism, Kyoto University Graduate School of Medicine, Kyoto; and* [3]*Department of Biochemistry, National Cardiovascular Center Research Institute, Osaka, Japan*

Submitted 13 December 2006; accepted in final form 22 June 2007

Iwakura H, Akamizu T, Ariyasu H, Irako T, Hosoda K, Nakao K, Kangawa K. Effects of ghrelin administration on decreased growth hormone status in obese animals. *Am J Physiol Endocrinol Metab* 293: E819–E825, 2007. First published June 26, 2007; doi:10.1152/ajpendo.00681.2006.—Obesity is characterized by markedly decreased ghrelin and growth hormone (GH) secretion. Ghrelin is a GH-stimulating, stomach-derived peptide that also has orexigenic action. Ghrelin supplement may restore decreased GH secretion in obesity, but it may worsen obesity by its orexigenic action. To reveal effects of ghrelin administration on obese animals, we first examined acute GH and orexigenic responses to ghrelin in three different obese and/or diabetic mouse models: *db/db* mice, mice on a high-fat diet (HFD mice), and Akita mice for comparison. GH responses to ghrelin were significantly suppressed in *db/db*, HFD, and Akita mice. Food intake of *db/db* and Akita mice were basally higher, and further stimulation of food intake by ghrelin was suppressed. Pituitary GH secretagogue receptor mRNA levels in *db/db* and HFD mice were significantly decreased, which may partly contribute to decreased GH response to ghrelin in these mice. In Akita mice for comparison, decreased hypothalamic GH-releasing hormone (GHRH) mRNA levels may be responsible for decreased GH response, since maximum GH response to ghrelin needs GHRH. When ghrelin was injected into HFD mice with GHRH coadministrated, GH responses to ghrelin were significantly emphasized. HFD mice injected with low-dose ghrelin and GHRH for 10 days did not show weight gain. These results indicate that low-dose ghrelin and GHRH treatment may restore decreased GH secretion in obesity without worsening obesity.

growth hormone secretagogue receptor; obesity; diabetes

IN HUMANS, OBESITY IS CHARACTERIZED by markedly decreased growth hormone (GH) production and secretion (3, 26). GH stimulates lipolysis and increases lean body mass, which may help to combat obesity. Decreased GH secretion in the context of obesity may promote additional fat deposition and promote weight gain (10). GH, however, does contribute to insulin resistance, which could worsen diabetes (7).

Ghrelin is a 28-amino acid peptide with unique acylation modification, which is essential for its biological action (14). Ghrelin was originally identified in the rat stomach as an endogenous ligand for an orphan receptor, which so far has been called GH secretagogue receptor (GHS-R) (14). Ghrelin is involved in a wide variety of functions, including regulation of GH release, gastric acid secretion, gastric motility, blood pressure, and cardiac output (4, 8, 18, 19, 23, 28). Ghrelin also has several metabolic functions, including orexigenic action (20, 22), reduction of insulin (5), and control of energy expenditure (24), which are all involved in the pathophysiology of adiposity or diabetes.

Plasma ghrelin level is suppressed in obesity (25), which may compensate for increased body weight by reducing its orexigenic activity, whereas low plasma ghrelin level may contribute to decreased GH secretion in obesity. Furthermore, Poykko et al. (21) reported that low plasma ghrelin level is associated with insulin resistance and incidence of type 2 diabetes.

To elucidate whether ghrelin supplementation can restore decreased GH secretion in obesity, we first determined acute GH and orexigenic responses to ghrelin in three different obese and/or diabetic mice models: *db/db* mice (a genetically obese mouse model with diabetes), mice on a high-fat diet (HFD; a diet-induced obese mouse model with moderate glucose intolerance), and Akita mice for comparison (an insulin-deprived diabetic nonobese mouse model) (29). Then, we determined how the ghrelin-GH system is modulated in the pituitaries and hypothalamuses of these animals. Last, we examined the effect of chronic ghrelin and GH-releasing hormone (GHRH) administration on diet-induced obesity.

MATERIALS AND METHODS

Experimental animals. Eight-week-old male *db/db* and control mice (misty) were purchased from CLEA Japan, (Tokyo, Japan). As a diet-induced model of obesity, 5-wk-old male C57BL/6J mice, purchased from Japan SLC (Shizuoka, Japan), were maintained on a HFD of 60% fat/kcal (Research Diets, New Brunswick, NJ) for 20 wk. Those maintained on a standard diet were used as control mice for HFD mice. Eight-week-old male Akita mice and C57BL/6J control mice were purchased from Japan SLC. Animals were maintained on standard rat food (CE-2, 352 kcal/100 g; CLEA Japan) with a 12:12-h light-dark cycle unless otherwise indicated. All experimental procedures were approved by the Kyoto University Graduate School of Medicine Committee on Animal Research.

Acute GH response to ghrelin and GHRH. Rat ghrelin (40, 120, and 360 μg/kg; Peptide Institute, Osaka, Japan), human GHRH (60 μg/kg; Mecasermin, Astellas Pharma, Tokyo, Japan), or saline was injected subcutaneously into mice on an ad libitum feeding schedule. Blood was collected from retroorbital veins 15 or 30 min after injection. Serum was isolated by centrifugation and stored at −20°C until assayed.

Measurements of hormones and free fatty acid levels. Serum GH levels were determined by rat growth hormone EIA kit (SPI bio,

Address for reprint requests and other correspondence: H. Iwakura, Ghrelin Research Project, Translational Research Center, Kyoto University Hospital, 54 Shogoin Kawahara-cho, Sakyo-ku, Kyoto 606-8507, Japan (e-mail: hiwaku@kuhp.kyoto-u.ac.jp).

The costs of publication of this article were defrayed in part by the payment of page charges. The article must therefore be hereby marked "*advertisement*" in accordance with 18 U.S.C. Section 1734 solely to indicate this fact.

Table 1. *Basal profiles of db/db mice on HFD and Akita mice*

	Con	*db/db*	Con	HFD	Con	Akita
Weight, g	23.1±0.25	42.3±0.20†	33.3±1.6	50.3±0.9†	24.6±0.5	23.1±0.5
Blood glucose, mg/dl	100.7±6.0	328.0±10.9†	05.5±5.5	125.1±4.1†	125.9±4.2	475.3±16.8†
Insulin, ng/ml	1.35±0.5	25.9±5.7†	3.6±1.1	28.0±6.9†	1.42±0.06	0.25±0.00†
IGF-I, ng/ml	659.9±19.9	764.1±41.5*	301.8±21.6	426.6±20.0†	416.4±21.4	415.8±17.9
FFA, mEq/l	0.78±0.04	1.68±0.11†	0.26±0.10	1.18±0.04	1.20±0.01	1.24±0.05
Ghrelin, fmol/ml	98.4±5.6	34.7±8.6†	164.9±7.5	67.2±10.6†	113.4±11.8	182.7±18.1†

Values are means ± SE. Con, control mice; HFD, mice on a high-fat diet; FFA, free fatty acids. *$P < 0.05$; †$P < 0.01$ compared with control mice or mice on a standard diet; $n = 7$.

Massy Cedes, France). Measurement of serum insulin concentrations was performed by ELISA using an ultrasensitive rat insulin kit (Morinaga, Yokohama, Japan). Serum insulin-like growth factor I (IGF-I) levels were measured using a mouse/rat IGF-I EIA kit (Diagnostic Systems Laboratories, Webster, TX). Serum free fatty acid (FFA) levels were measured by NEFA C test (Wako Pure Chemical Industries, Osaka, Japan).

Measurements of plasma ghrelin concentrations. Measurement of plasma ghrelin levels was performed as reported previously (12). Briefly, blood was drawn from the retroorbital vein after an overnight fast and then immediately transferred to chilled siliconized glass tubes containing Na_2EDTA (1 mg/ml) and aprotinin (1,000 KIU/ml; Ohkura Pharmaceutical, Kyoto, Japan) and centrifuged at 4°C. Immediately after the plasma was separated, hydrochloric acid was added to samples at final concentration of 0.1 N. Plasma was immediately frozen and stored at −80°C until assay. Plasma ghrelin concentrations were determined using an active ghrelin ELISA kit that recognizes *n*-octanoylated ghrelin (Mitsubishi Kagaku Iatron, Tokyo, Japan) (1).

Real-time quantitative RT-PCR. Total RNA was extracted from the pituitary and hypothalamus using a Sepasol RNA kit (Nacalai Tesque, Kyoto, Japan). Reverse transcription (RT) was performed in the presence of random hexamers with SuperScript II reverse transcriptase (Invitrogen, Carlsbad, CA). Real-time quantitative PCR was performed using an ABI PRISM 7500 Sequence Detection System (Applied Biosystems, Foster City, CA), using the following primers and TaqMan probes: mouse GH sense, 5′-AAGAGTTCGAGCGTGCCTACA-3′, and antisense, 5′-GAAGCAATTCCATGTCGGTTC-3′, with the TaqMan probe, 5′-CCATTCAGAATGCCCAGGCTGCTTTC-3′; mouse GHRH receptor (GHRH-R) sense, 5′-GCCCTTGGAACTGTTAACCA-3′, and antisense, 5′-GCAACCAGGATGGCAATAGC-3′, with the TaqMan probe, 5′-AGCATCTCCATTGTAGCCCTCTGCGTG-3′; mouse GHS-R sense, 5′-CACCAACCTCTACCTATCCAGCAT-3′, and antisense, 5′-CTGACAAACTGGAAGAGTTTGCA-3′, with the TaqMan probe, 5′-TCCGATCTGCTCATCTTCCTGTGCATG-3′; mouse ghrelin sense, 5′-GCATGCTCTGGATGGACATG-3′, and antisense, 5′-TGGTGGCTTCTTGGATTCCT-3′, with the TaqMan probe, 5′-AGCCCAGAGCACCAGAAAGCCCA-3′; mouse somatostatin receptor (SSTR)2 sense, 5′-GGTCAAGGCAGACAATTCACAA -3′, and antisense, 5′-GTGTTAGCACACATACACACAGGACTT -3′, with the TaqMan probe, 5′-CGGCAGAAACCGGAAAAACCAAAACTAAAT -3′; mouse SSTR5 sense, 5′-CGCTGCCTGACCGCTAAGTA-3′, and antisense, 5′-GCTCACAGAGGTTGGCTCACA-3′, with the TaqMan probe, 5′-CTGCACAGGAGAGGTCTCCACGGCT-3′; mouse GHRH sense, 5′-AGGATGCAGCGACACGTAGA-3′, and antisense, 5′-TCTCCCCTTGCTTGTTCATGA-3′, with the TaqMan probe, 5′-CCACCAACTACAGGAAACTCCTGAGCCA-3′. The mRNA expression in each gene was normalized to that of 18s ribosomal RNA.

Chronic administration of ghrelin and GHRH. Mice on a HFD (HFD mice) or a standard diet (control mice) for 20 wk were injected with 40 μg/kg ghrelin and 60 μg/kg GHRH twice daily for 10 days. Before and after treatment, blood samples were collected and body weights measured. Fat body mass and lean body mass of mice were measured by Latheta LTC-100 (Aloka, Tokyo, Japan) under pentobarbital anesthesia.

Statistical analysis. All values were expressed as means ± SE. The statistical significance of the differences in mean values was assessed by two-way ANOVA or Student's *t*-test as appropriate.

RESULTS

Basal profiles of *db/db*, HFD, and Akita mice are listed in Table 1. *Db/db* and HFD mice showed significantly higher weights, blood glucose, serum insulin, and serum IGF-I levels and significantly lower plasma ghrelin levels than those seen in control mice (Table 1), although the elevation of blood glucose was less severe in HFD mice. Although serum FFA levels of *db/db* mice were significantly higher than those of control mice, those of HFD mice were comparable with those of control mice (Table 1). Although Akita mice demonstrated significantly higher blood glucose levels as either *db/db* mice or HFD mice, Akita mice displayed significantly lower body weights and serum insulin levels and higher plasma ghrelin levels than those seen in control mice (Table 1).

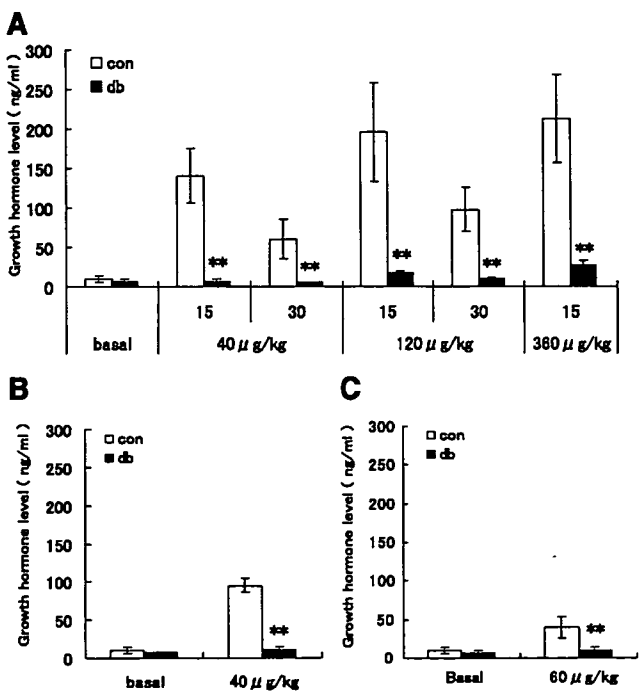

Fig. 1. Growth hormone (GH) responses to ghrelin in *db/db* mice. *A*: serum GH levels 15 or 30 min after sc injection of ghrelin into *db/db* (db) or control (con) mice. *B*: serum GH levels 15 min after iv ghrelin injection into db or con mice. *C*: serum GH levels 15 min after sc injection of GH-releasing hormone (GHRH). **$P < 0.01$.

We first examined acute GH responses to ghrelin in *db/db*, HFD, and Akita mice. GH responses to ghrelin in *db/db* mice were markedly lower than those observed in control mice at any dose (40, 120, or 360 μg/kg; Fig. 1*A*). Thirty minutes after ghrelin injection (40 or 120 μg/kg) of *db/db* mice, serum GH levels tended to be even lower than those at 15 min (Fig. 1*A*), indicating that low GH levels at 15 min were not due to delayed response. GH responses at 15 min after intravenous injection of ghrelin were also decreased in *db/db* mice (Fig. 1*B*), indicating that the disturbed GH responses observed in *db/db* mice were not due to the malabsorption of ghrelin caused by fat deposition at the subcutaneous injection site. GH responses to GHRH (60 μg/kg) were also decreased in *db/db* mice (Fig. 1*C*). As in *db/db* mice, GH levels at 15 min after subcutaneous ghrelin injection (40, 120, and 360 μg/kg) in HFD mice were significantly lower than those seen in control mice (Fig. 2*A*). GH responses to GHRH (60 μg/kg) also tended to be decreased (Fig. 2*B*). Although GH levels in Akita mice were not significantly different from those in control mice measured at 15 min after 40 μg/kg sc injection of ghrelin, those measured after a higher dose of ghrelin (120 and 360 μg/kg) were significantly lower than those in control mice (Fig. 3*A*). GH responses to GHRH (60 μg/kg) also tended to be decreased in Akita mice (Fig. 3*B*).

We then measured 1-h food intake stimulated by ghrelin in *db/db* and Akita mice. In control mice, a 40 μg/kg sc ghrelin injection evoked about threefold greater food intake than that

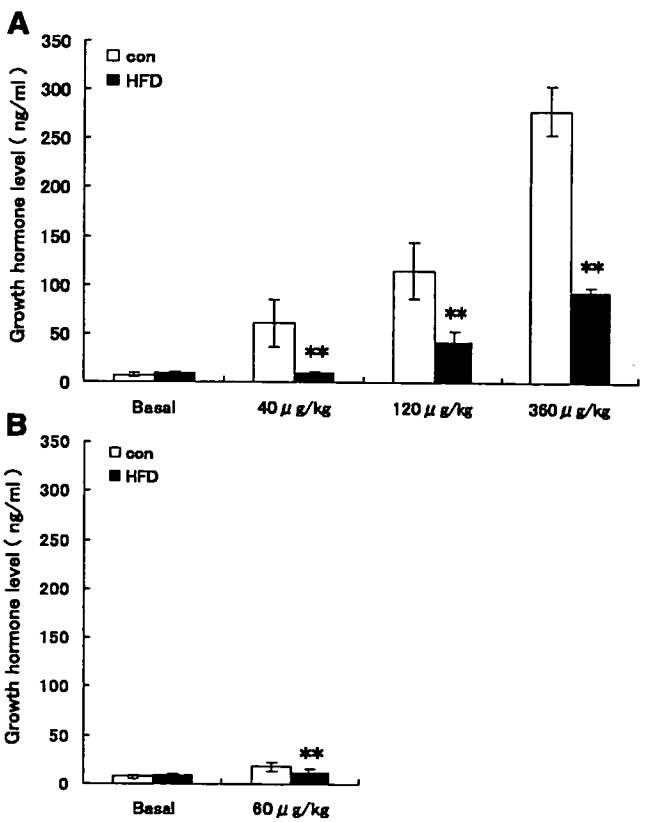

Fig. 2. GH responses to ghrelin in a diet-induced obesity mouse model. *A*: serum GH levels 15 min after sc injection of ghrelin into mice on a high-fat diet (HFD) or con mice. *B*: serum GH levels 15 min after GHRH sc injection. $^{**}P < 0.01$ compared with controls; $n = 7$.

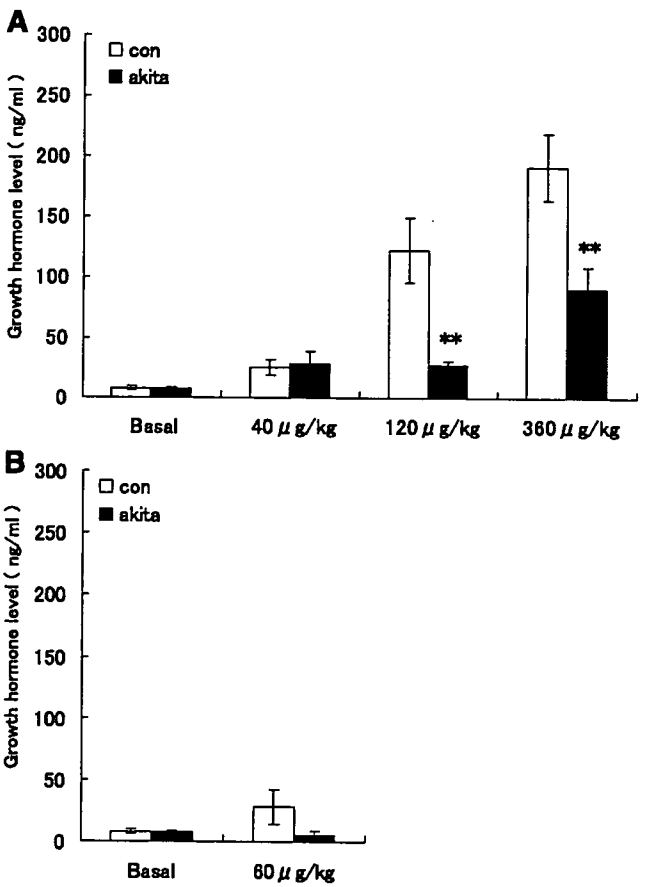

Fig. 3. GH responses to ghrelin in Akita mice. *A*: serum GH levels 15 min after sc injection of ghrelin into Akita or con mice. *B*: serum GH levels 15 min after sc injection of GHRH. $^{**}P < 0.01$ compared with control; $n = 7$.

induced by saline injection (saline vs. ghrelin: 0.09 ± 0.04 vs. 0.28 ± 0.01 g, $P < 0.05$, $n = 7$; Fig. 4*A*). Ghrelin stimulated additional food intake in a dose-dependent manner in control mice, as demonstrated by the ratio of food intake evoked by ghrelin to that induced by saline (Fig. 4*A*). In *db/db* mice, basal food intake was higher than that of control mice (0.22 ± 0.05 vs. 0.07 ± 0.02 g, $P < 0.05$, $n = 7$). Although sc injection of 40 μg/kg ghrelin into *db/db* mice did not stimulate food intake significantly (saline vs. ghrelin: 0.30 ± 0.11 vs. 0.18 ± 0.04 g, $P = 0.30$, $n = 7$), higher doses of ghrelin (360 μg/kg), however, were able to stimulate food intake (saline vs. ghrelin: 0.14 ± 0.08 vs. 0.39 ± 0.04 g, $P < 0.05$, $n = 7$). Although higher ghrelin stimulated food intake in *db/db* mice, the extent of stimulation as demonstrated by the ratio of ghrelin-induced food intake (40 and 360 μg/kg) to that by saline was significantly smaller than that in control mice (Fig. 4*A*). In Akita mice, basal food intake was higher than that of control mice (0.28 ± 0.01 vs. 0.15 ± 0.02 g, $P < 0.05$, $n = 7$), and no further stimulation of food intake by ghrelin was observed (Fig. 4*B*).

We then measured the mRNA expression of ghrelin-GH system in pituitaries and hypothalamuses of *db/db*, HFD, and Akita mice (Fig. 5). Pituitary mRNA levels of GHS-R were significantly lower in *db/db* and HFD mice, whereas those in Akita mice were significantly higher compared with their

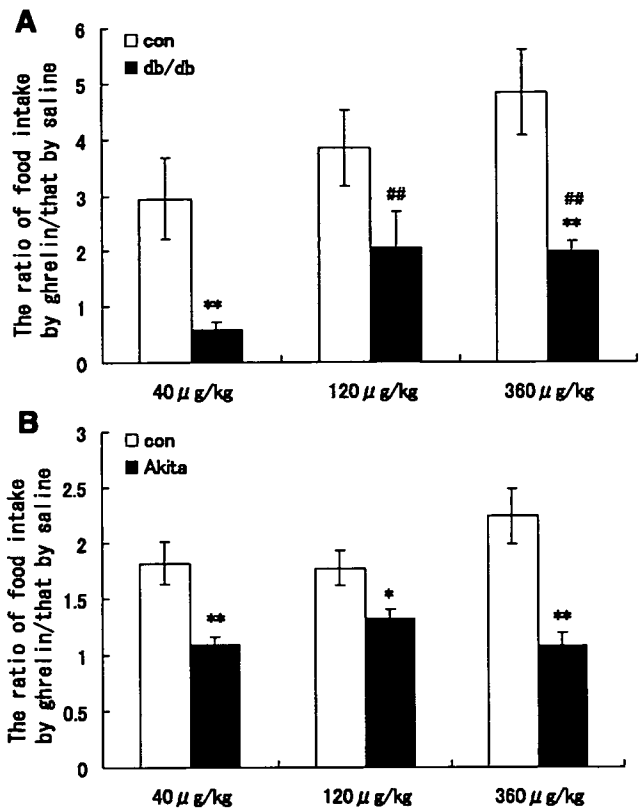

Fig. 4. Food intake stimulated by sc ghrelin injection. *A*: the ratio of 1-h food intake after sc ghrelin injection to that observed after sc saline injection in db and con mice. *B*: the ratio of the food intake observed for 1 h after sc ghrelin injection to that seen after saline injection for Akita and con mice. $*P < 0.05$; $**P < 0.01$ compared with control; $\#\#P < 0.01$ compared with 40 μg/kg; $n = 7$.

control mice (Fig. 5*A*). Pituitary mRNA levels of ghrelin were significantly lower in *db/db* mice, whereas those in Akita mice were significantly higher (Fig. 5*A*). Pituitary mRNA levels of GH were significantly lower in *db/db* and HFD mice and tended to be lower in Akita mice (Fig. 5*A*). Pituitary mRNA levels of SSTR2 were significantly higher in *db/db* mice, whereas they were not significantly changed in HFD and Akita mice (Fig. 5*A*). Pituitary mRNA levels of SSTR5 were significantly lower in Akita mice, whereas those levels were not significantly changed in *db/db* and HFD mice (Fig. 5*A*). There were no significant changes in the expression levels of GHRH-R in pituitaries of these mice (Fig. 5*A*). In hypothalamus, GHS-R and GHRH mRNA levels were significantly higher and lower, respectively, in Akita mice (Fig. 5*B*). Ghrelin mRNA levels were significantly lower in hypothalamus of HFD mice (Fig. 5*B*).

Finally, we examined the effect of chronic ghrelin injection to HFD mice. To maximize GH-stimulating activity of ghrelin and to minimize orexigenic action of ghrelin, we first examined GH responses to low-dose ghrelin with GHRH coadministration in HFD mice. Acute GH responses to ghrelin were significantly potentiated by coadministration of GHRH even at the lowest dose in HFD mice (Fig. 6*A*). By 10 days of twice daily injections of saline or ghrelin and GHRH, both control and HFD mice lose weight by ~6–8%. This weight reduction might be due to stress of twice daily injection, which is usually covered by growth in younger mice. Control mice treated with ghrelin and GHRH tended to take in more food than those with saline (Fig. 6*C*). Fat masses were more preserved in the ghrelin- and GHRH-treated groups than in the saline-treated group in control mice (Fig. 6, *B*, *D*, and *E*), although percent body weight and percent lean body mass changes were comparable between the saline-treated and the ghrelin- and GHRH-treated group in control mice. In HFD mice, food intake, percent body weight change, and percent lean body mass change were comparable between the saline-treated group and the ghrelin- and GHRH-treated groups (Fig. 6, *B*, *D*, and *E*). In contrast to control mice, fat mass tended to even be decreased in the ghrelin and GHRH group than in the saline-treated group in HFD mice (Fig. 6*D*). In both control and HFD mice, blood glucose, serum insulin, and serum IGF-I levels of the ghrelin- and GHRH-treated group were not significantly different from those of the saline-treated group (Fig. 6, *F*, *G*, and *H*).

DISCUSSION

We have demonstrated that GH responses to ghrelin are decreased in both genetic and diet-induced mouse models of obesity. Recently, Luque and Kineman (15) reported that plasma GH levels acquired by random sampling without stimulation in *ob/ob* mice and HFD mice tended to be lower than

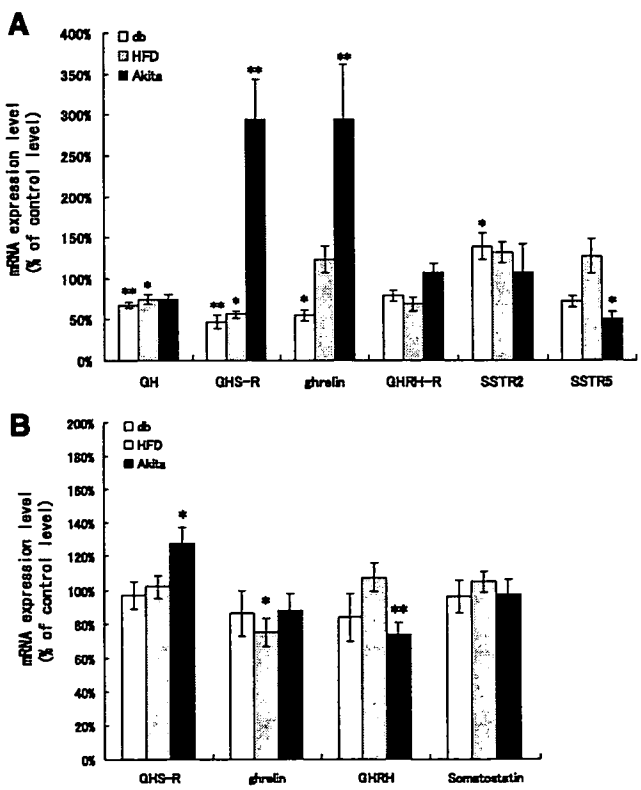

Fig. 5. The mRNA expression levels in the pituitaries or hypothalamuses of db mice, mice on a HFD, and Akita mice. *A*: the mRNA expression levels of GH, GH secretagogue receptor (GHS-R), ghrelin, GH-releasing hormone receptor (GHRH-R), somatostatin receptor (SSTR)2, and SSTR5 in the pituitaries of db, HFD, and Akita mice. *B*: the mRNA expression levels of GHS-R, ghrelin, GHRH, and somatostatin in the hypothalamuses of db, HFD, and Akita mice. Data were presented as % of the level seen in control mice. $*P < 0.05$; $**P < 0.01$ compared with control; $n = 14$.

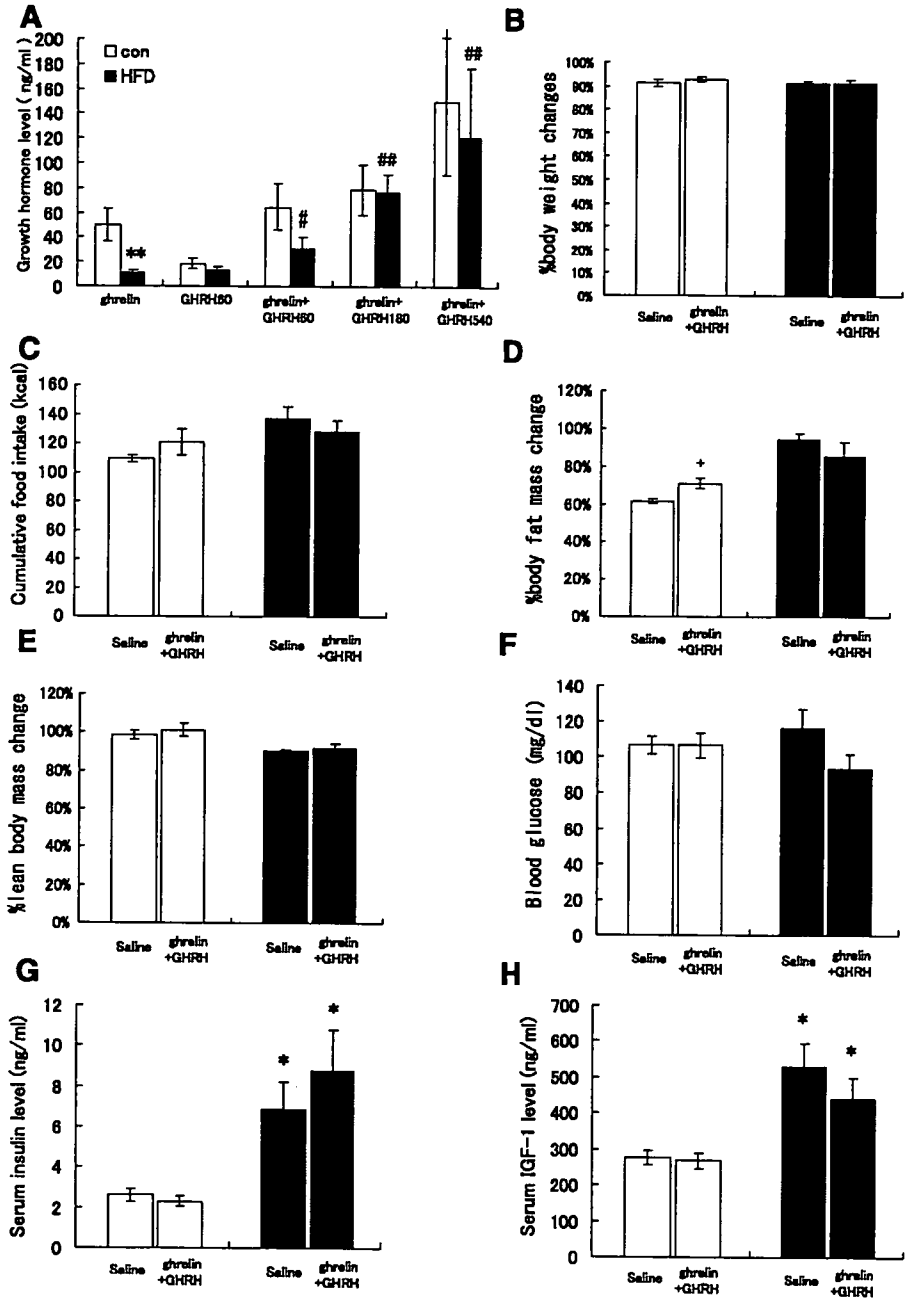

Fig. 6. Chronic treatment of ghrelin and GHRH on mice on a HFD. *A*: serum GH levels 15 or 30 min after sc injection of 40 μg/kg ghrelin or 60 μg/kg GHRH or ghrelin and GHRH (60, 180, 540 μg/kg) into HFD or con mice. %Body weight (*B*), fat mass (*D*), and lean body mass (*E*) changes before and after treatment of 40 μg/kg ghrelin and 60 μg/kg GHRH or saline for 10 days in control mice (open bars) or mice on a HFD (filled bars). *C*: cumulative food intake for 10 days. Blood glucose (*F*), serum insulin level (*G*), and serum IGF-I level (*H*) after 10 days administration of ghrelin and GHRH. $*P < 0.05$; $**P < 0.01$ compared with control; $\#P < 0.05$; $\#\#P < 0.01$ compared with ghrelin; $+P < 0.05$ compared with saline; $n = 7$.

those seen in control mice. Because GH secretion is pulsatile, it is difficult to compare GH values obtained by random sampling in the absence of stimulation. For this reason, we could not detect any significant difference in basal GH values between *db/db* or HFD and control mice. Following ghrelin or GHRH stimulation, however, we clearly observed a severe impairment in GH secretions by obese mice. Alvarez-Castro et al. (2) previously reported that GH responses to ghrelin were decreased in obese human subjects compared with those seen in normal controls; although reduced, these responses to ghrelin were greater in magnitude than those observed following GHRH treatment in obese human subjects. Our observations in mice were consistent with these data obtained in humans, which verify the use of *db/db* and HFD mice as experimental animal models for ghrelin treatment for obesity.

We also demonstrated that GH responses to ghrelin are decreased in Akita mice. As far as we know, this is the first report on the GH responses to ghrelin in insulin-deprived mice. In humans with insulin-deprived diabetes, it is well known (11) that basal GH is elevated and that GH response to provocative tests, including GHRH or GHS administration, is exaggerated. Thus discrepancy between human and mouse GH response to ghrelin in insulin-deprived status exist.

We demonstrated that GHS-R mRNA levels were decreased in the pituitaries of *db/db* and HFD mice. Ghrelin does stimulate GH release from rat pituitary in vitro (14), but maximal

response of GH to ghrelin requires the existence of GHRH (9). Kamegai et al. (13) reported that pituitary ghrelin regulates GH secretion by modulating pituitary response to GHRH. The decreased expression of GHS-R in pituitary in *db/db* and HFD mice might contribute to suppressed GH response to ghrelin by attenuating the pituitary response to GHRH. Of course, decreased mRNA levels of GH in pituitary or, as reported in human (6, 16), elevated serum IGF-I or FFA levels in these mice might also contribute to suppressed GH responses.

Although GH responses to ghrelin were also decreased in Akita mice, the pituitary mRNA levels of GHS-R were significantly higher than those seen in control mice, indicating that pituitary GHS-R did not contribute to decreased GH responses. GHRH mRNA expression levels in hypothalamus of Akita mice were significantly lower compared with those of control mice. This reduction of GHRH mRNA levels may be responsible for decreased GH responses to ghrelin in Akita mice. Ghrelin stimulates GHRH secretion from the hypothalamus (27). And recently, Mano-Otagiri et al. (17) reported that GHS-R signaling upregulates hypothalamic GHRH expression. Although plasma ghrelin levels were significantly higher in Akita mice than those displayed by control mice, GHRH mRNA expression levels in hypothalamus of Akita mice were significantly decreased. In addition, the food intake of Akita mice was significantly elevated at baseline and was not stimulated by ghrelin any further. These results indicate the existence of ghrelin unresponsiveness in postreceptor level in hypothalamus.

In the chronic treatment experiment, ghrelin and GHRH treatment for 10 days tended to stimulate food intake and showed fat-sparing effect in control mice. In contrast, HFD mice injected with ghrelin and GHRH tended to decrease more fat mass compared with those treated with saline, which may be due to restored GH secretion and suppressed orexigenic response to ghrelin. In this setting, blood glucose and serum insulin levels did not change by ghrelin and GHRH treatment in HFD mice. This may be explained by the fact that the change in fat mass was only subtle and that lean body mass did not change by ghrelin and GHRH treatment. These results indicate that low-dose ghrelin and GHRH supplementation at least do not worsen obesity and metabolic status and that it may at least partially restore suppressed GH secretion.

In the current experiment, IGF-I levels were higher in HFD mice after chronic treatment of ghrelin and GHRH. Since IGF-I levels of the saline-treated group of HFD mice were also higher than those of control mice, this elevation seems to reflect nutritional status between HFD and control mice.

In conclusion, we demonstrated that acute GH responses to ghrelin were suppressed in both genetic and diet-induced mouse models of obesity. The decreased pituitary levels of GHS-R mRNA may contribute to suppression of GH response. We also demonstrated that acute GH responses to ghrelin were suppressed in Akita mice, an insulin-deprived diabetic mouse model. Decreased GHRH mRNA levels in hypothalamus and the lack of stimulation of food intake by ghrelin indicate the involvement of hypothalamus in the mechanism of suppressed GH response to ghrelin in Akita mice. These results indicate that suppressed GH response to ghrelin has a different mechanism in obese and insulin-resistant mice and insulin-deprived diabetic animals. In addition, HFD mice injected with ghrelin and GHRH showed potentiated GH responses. Chronic treatment of low-dose ghrelin and GHRH did not promote fat deposition in HFD mice. These results indicate that low-dose ghrelin and GHRH administration at least does not worsen obesity and that it may restore suppressed GH secretion.

ACKNOWLEDGMENTS

We thank Hitomi Hiratani, Chieko Ishimoto, Naoko Takehisa, Kozue Fukuda, and Chinami Shiraiwa for excellent technical assistance.

GRANTS

This study was supported by funds from the Ministry of Education, Culture, Sports, Science, and Technology of Japan and the Ministry of Health, Labour, and Welfare of Japan.

REFERENCES

1. **Akamizu T, Shinomiya T, Irako T, Fukunaga M, Nakai Y, Kangawa K.** Separate measurement of plasma levels of acylated and desacyl ghrelin in healthy subjects using a new direct ELISA assay. *J Clin Endocrinol Metab* 90: 6–9, 2005.
2. **Alvarez-Castro P, Isidro ML, Garcia-Buela J, Leal-Cerro A, Broglio F, Tassone F, Ghigo E, Dieguez C, Casanueva FF, Cordido F.** Marked GH secretion after ghrelin alone or combined with GH-releasing hormone (GHRH) in obese patients. *Clin Endocrinol (Oxf)* 61: 250–255, 2004.
3. **Argente J, Caballo N, Barrios V, Pozo J, Munoz MT, Chowen JA, Hernandez M.** Multiple endocrine abnormalities of the growth hormone and insulin-like growth factor axis in prepubertal children with exogenous obesity: effect of short- and long-term weight reduction. *J Clin Endocrinol Metab* 82: 2076–2083, 1997.
4. **Arvat E, Di Vito L, Broglio F, Papotti M, Muccioli G, Dieguez C, Casanueva FF, Deghenghi R, Camanni F, Ghigo E.** Preliminary evidence that Ghrelin, the natural GH secretagogue (GHS)-receptor ligand, strongly stimulates GH secretion in humans. *J Endocrinol Invest* 23: 493–495, 2000.
5. **Broglio F, Arvat E, Benso A, Gottero C, Muccioli G, Papotti M, van der Lely AJ, Deghenghi R, Ghigo E.** Ghrelin, a natural GH secretagogue produced by the stomach, induces hyperglycemia and reduces insulin secretion in humans. *J Clin Endocrinol Metab* 86: 5083–5086, 2001.
6. **Cordido F, Fernandez T, Martinez T, Penalva A, Peino R, Casanueva FF, Dieguez C.** Effect of acute pharmacological reduction of plasma free fatty acids on growth hormone (GH) releasing hormone-induced GH secretion in obese adults with and without hypopituitarism. *J Clin Endocrinol Metab* 83: 4350–4354, 1998.
7. **Cutfield WS, Wilton P, Bennmarker H, Albertsson-Wikland K, Chatelain P, Ranke MB, Price DA.** Incidence of diabetes mellitus and impaired glucose tolerance in children and adolescents receiving growth-hormone treatment. *Lancet* 355: 610–613, 2000.
8. **Date Y, Murakami N, Kojima M, Kuroiwa T, Matsukura S, Kangawa K, Nakazato M.** Central effects of a novel acylated peptide, ghrelin, on growth hormone release in rats. *Biochem Biophys Res Commun* 275: 477–480, 2000.
9. **Fintini D, Alba M, Schally AV, Bowers CY, Parlow AF, Salvatori R.** Effects of combined long-term treatment with a growth hormone-releasing hormone analogue and a growth hormone secretagogue in the growth hormone-releasing hormone knock out mouse. *Neuroendocrinology* 82: 198–207, 2005.
10. **Furuhata Y, Kagaya R, Hirabayashi K, Ikeda A, Chang KT, Nishihara M, Takahashi M.** Development of obesity in transgenic rats with low circulating growth hormone levels: involvement of leptin resistance. *Eur J Endocrinol* 143: 535–541, 2000.
11. **Giustina A, Veldhuis JD.** Pathophysiology of the neuroregulation of growth hormone secretion in experimental animals and the human. *Endocr Rev* 19: 717–797, 1998.
12. **Iwakura H, Hosoda K, Son C, Fujikura J, Tomita T, Noguchi M, Ariyasu H, Takaya K, Masuzaki H, Ogawa Y, Hayashi T, Inoue G, Akamizu T, Hosoda H, Kojima M, Itoh H, Toyokuni S, Kangawa K, Nakao K.** Analysis of rat insulin II promoter-ghrelin transgenic mice and rat glucagon promoter-ghrelin transgenic mice. *J Biol Chem* 280: 15247–15256, 2005.
13. **Kamegai J, Tamura H, Shimizu T, Ishii S, Tatsuguchi A, Sugihara H, Oikawa S, Kineman RD.** The role of pituitary ghrelin in growth hormone (GH) secretion: GH-releasing hormone-dependent regulation of pituitary

ghrelin gene expression and peptide content. *Endocrinology* 145: 3731–3738, 2004.
14. **Kojima M, Hosoda H, Date Y, Nakazato M, Matsuo H, Kangawa K.** Ghrelin is a growth-hormone-releasing acylated peptide from stomach. *Nature* 402: 656–660, 1999.
15. **Luque RM, Kineman RD.** Impact of obesity on the growth hormone (GH)-axis: evidence for a direct inhibitory effect of hyperinsulinemia on pituitary function. *Endocrinology* 147: 2754–2763, 2006.
16. **Maccario M, Tassone F, Gianotti L, Lanfranco F, Grottoli S, Arvat E, Muller EE, Ghigo E.** Effects of recombinant human insulin-like growth factor I administration on the growth hormone (gh) response to GH-releasing hormone in obesity. *J Clin Endocrinol Metab* 86: 167–171, 2001.
17. **Mano-Otagiri A, Nemoto T, Sekino A, Yamauchi N, Shuto Y, Sugihara H, Oikawa S, Shibasaki T.** Growth hormone-releasing hormone (GHRH) neurons in the arcuate nucleus (Arc) of the hypothalamus are decreased in transgenic rats whose expression of ghrelin receptor is attenuated: evidence that ghrelin receptor is involved in the up-regulation of GHRH expression in the arc. *Endocrinology* 147: 4093–4103, 2006.
18. **Masuda Y, Tanaka T, Inomata N, Ohnuma N, Tanaka S, Itoh Z, Hosoda H, Kojima M, Kangawa K.** Ghrelin stimulates gastric acid secretion and motility in rats. *Biochem Biophys Res Commun* 276: 905–908, 2000.
19. **Nagaya N, Uematsu M, Kojima M, Ikeda Y, Yoshihara F, Shimizu W, Hosoda H, Hirota Y, Ishida H, Mori H, Kangawa K.** Chronic administration of ghrelin improves left ventricular dysfunction and attenuates development of cardiac cachexia in rats with heart failure. *Circulation* 104: 1430–1435, 2001.
20. **Nakazato M, Murakami N, Date Y, Kojima M, Matsuo H, Kangawa K, Matsukura S.** A role for ghrelin in the central regulation of feeding. *Nature* 409: 194–198, 2001.
21. **Poykko SM, Kellokoski E, Horkko S, Kauma H, Kesaniemi YA, Ukkola O.** Low plasma ghrelin is associated with insulin resistance, hypertension, and the prevalence of type 2 diabetes. *Diabetes* 52: 2546–2553, 2003.
22. **Shintani M, Ogawa Y, Ebihara K, Aizawa-Abe M, Miyanaga F, Takaya K, Hayashi T, Inoue G, Hosoda K, Kojima M, Kangawa K, Nakao K.** Ghrelin, an endogenous growth hormone secretagogue, is a novel orexigenic peptide that antagonizes leptin action through the activation of hypothalamic neuropeptide Y/Y1 receptor pathway. *Diabetes* 50: 227–232, 2001.
23. **Takaya K, Ariyasu H, Kanamoto N, Iwakura H, Yoshimoto A, Harada M, Mori K, Komatsu Y, Usui T, Shimatsu A, Ogawa Y, Hosoda K, Akamizu T, Kojima M, Kangawa K, Nakao K.** Ghrelin strongly stimulates growth hormone release in humans. *J Clin Endocrinol Metab* 85: 4908–4911, 2000.
24. **Tschop M, Smiley DL, Heiman ML.** Ghrelin induces adiposity in rodents. *Nature* 407: 908–913, 2000.
25. **Tschop M, Weyer C, Tataranni PA, Devanarayan V, Ravussin E, Heiman ML.** Circulating ghrelin levels are decreased in human obesity. *Diabetes* 50: 707–709, 2001.
26. **Veldhuis JD, Iranmanesh A, Ho KK, Waters MJ, Johnson ML, Lizarralde G.** Dual defects in pulsatile growth hormone secretion and clearance subserve the hyposomatotropism of obesity in man. *J Clin Endocrinol Metab* 72: 51–59, 1991.
27. **Wren AM, Small CJ, Fribbens CV, Neary NM, Ward HL, Seal LJ, Ghatei MA, Bloom SR.** The hypothalamic mechanisms of the hypophysiotropic action of ghrelin. *Neuroendocrinology* 76: 316–324, 2002.
28. **Wren AM, Small CJ, Ward HL, Murphy KG, Dakin CL, Taheri S, Kennedy AR, Roberts GH, Morgan DG, Ghatei MA, Bloom SR.** The novel hypothalamic peptide ghrelin stimulates food intake and growth hormone secretion. *Endocrinology* 141: 4325–4328, 2000.
29. **Yoshioka M, Kayo T, Ikeda T, Koizumi A.** A novel locus, Mody4, distal to D7Mit189 on chromosome 7 determines early-onset NIDDM in nonobese C57BL/6 (Akita) mutant mice. *Diabetes* 46: 887–894, 1997.

Am J Physiol Renal Physiol 293: F1363–F1372, 2007.
First published August 15, 2007; doi:10.1152/ajprenal.00205.2007.

Expression of CCN1 (CYR61) in developing, normal, and diseased human kidney

Kazutomo Sawai,[1,6] Masashi Mukoyama,[1] Kiyoshi Mori,[1] Masato Kasahara,[1] Masao Koshikawa,[1] Hideki Yokoi,[1] Tetsuro Yoshioka,[1] Yoshihisa Ogawa,[1] Akira Sugawara,[1] Hiroyuki Nishiyama,[2] Shigehito Yamada,[3] Takashi Kuwahara,[4] Moin A. Saleem,[5] Kohei Shiota,[3] Osamu Ogawa,[2] Mikiya Miyazato,[6] Kenji Kangawa,[6] and Kazuwa Nakao[1]

Departments of [1]Medicine and Clinical Science and [2]Urology, and [3]Congenital Anomaly Research Center, Kyoto University Graduate School of Medicine, Kyoto; [4]Department of Nephrology, Osaka Saiseikai Nakatsu Hospital, Osaka; [5]Children's Renal Unit, University of Bristol, Bristol, United Kingdom; [6]Department of Biochemistry, National Cardiovascular Center Research Institute, Osaka, Japan

Submitted 30 April 2007; accepted in final form 6 August 2007

Sawai K, Mukoyama M, Mori K, Kasahara M, Koshikawa M, Yokoi H, Yoshioka T, Ogawa Y, Sugawara A, Nishiyama H, Yamada S, Kuwahara T, Saleem MA, Shiota K, Ogawa O, Miyazato M, Kangawa K, Nakao K. Expression of CCN1 (CYR61) in developing, normal, and diseased human kidney. *Am J Physiol Renal Physiol* 293: F1363–F1372, 2007. First published August 15, 2007; doi:10.1152/ajprenal.00205.2007.—CCN1 (cysteine-rich protein 61; Cyr61) is an extracellular matrix-associated signaling molecule that functions in cell migration, adhesion, and differentiation. We previously reported that CCN1 is induced at podocytes in rat anti-Thy-1 glomerulonephritis, a well-known model of reversible glomerular injury, but its expression and significance in the human kidney remain totally unknown (Sawai K, Mori K, Mukoyama M, Sugawara A, Suganami T, Koshikawa M, Yahata K, Makino H, Nagae T, Fujinaga Y, Yokoi H, Yoshioka T, Yoshimoto A, Tanaka I, Nakao K. *J Am Soc Nephrol* 14: 1154–1163, 2003). Here we report that, in the human kidney, CCN1 expression was confined to podocytes in normal adult and embryonic glomeruli from the capillary loop stage. Podocyte CCN1 expression was decreased in IgA nephropathy, diabetic nephropathy, and membranous nephropathy, whereas it remained unchanged in minimal change disease and focal segmental glomerulosclerosis. Downregulation of CCN1 was significantly greater in diseased kidneys with severe mesangial expansion. CCN1 protein was also localized in the thick ascending limb of Henle's loop, distal and proximal tubules, and collecting ducts, which was not altered in diseased kidneys. In vitro, recombinant CCN1 protein enhanced endothelial cell adhesion, whereas it prominently inhibited mesangial cell adhesion. CCN1 also completely suppressed mesangial cell migration, suggesting its role as a mesangial-repellent factor. In cultured podocytes, CCN1 markedly induced the expression of cyclin-dependent kinase inhibitor $p27^{Kip1}$ as well as synaptopodin in a dose-dependent manner and suppressed podocyte migration. These data indicate that CCN1 is expressed in podocytes, can act on glomerular cells to modulate glomerular remodeling, and is downregulated in diseased kidneys, suggesting that impairment of CCN1 expression in podocytes may contribute to the progression of glomerular disease with mesangial expansion.

podocyte; glomerular visceral epithelial cell; cysteine-rich protein 61; mesangial cell; synaptopodin

CYSTEINE-RICH PROTEIN 61 (Cyr61; also known as CCN1) is a secreted, 42-kDa, angiogenic protein belonging to the family of CCN proteins, which contains Cyr61 (CCN1), connective tissue growth factor (CTGF; CCN2), nephroblastoma overexpressed (Nov; CCN3), and Wnt-induced secreted proteins (WISP)-1, -2, and -3 (CCN4, 5, and 6, respectively) (3, 19, 28). CCN proteins are associated with extracellular matrix, interact with various integrins, and mediate a variety of biological actions including cell adhesion, migration, and differentiation, and induce angiogenesis both in vitro and in vivo (2, 3, 13, 19, 28). Among them, CCN1 is essential for vessel bifurcation during development, and most CCN1-null mice suffer embryonic death between embryonic (E) days *E11.5* and *E14.5* due to vessel malformation in the placenta and within embryos (22). In adults, CCN1 is suggested to be involved in skin wound healing (4) and adaptation to cardiovascular stress such as ischemia and pressure overload (11), but its role in the kidney remains undefined.

We have recently reported that CCN1 is prominently induced at podocytes during glomerular regeneration in rat anti-Thy-1 glomerulonephritis (Thy-1 GN) (32), a well-known model of reversible glomerulonephritis. CCN1 expression in podocytes was potently stimulated by transforming growth factor-β (TGF-β) and platelet-derived growth factor (PDGF) (32). CCN1 was also expressed in the proximal straight tubules, where its expression was not altered during Thy-1 GN. Conditioned medium from CCN1-overexpressing cells inhibited mesangial cell migration without affecting cell proliferation (32). From these results, we speculated that CCN1 secreted from podocytes might enhance glomerular repair in Thy-1 GN by protecting the glomerular capillary lumen from being occluded by migrating mesangial cells. However, the expression and the pathophysiological significance of CCN1 in human kidneys remain to be elucidated.

In this study, we investigated CCN1 expression in fetal and adult human kidneys, as well as in various glomerular diseases. Furthermore, we studied the effects of CCN1 on mesangial cells and podocytes in vitro. Our data indicate that CCN1 expression in podocytes is decreased in diseased kidneys with mesangial expansion, suggesting that impairment of CCN1 expression may contribute to the progression of various glomerular diseases.

Address for reprint requests and other correspondence: M. Mukoyama, Dept. of Medicine and Clinical Science, Kyoto Univ. Graduate School of Medicine, 54 Shogoin Kawahara-cho, Sakyo-ku, Kyoto 606-8507, Japan (e-mail: muko@kuhp.kyoto-u.ac.jp).

The costs of publication of this article were defrayed in part by the payment of page charges. The article must therefore be hereby marked "*advertisement*" in accordance with 18 U.S.C. Section 1734 solely to indicate this fact.

Table 1. *Clinical parameters of the patients*

Diagnosis	*n*	Gender (M/F)	Age, yr	sCr, mg/dl	BUN, mg/dl	Urinary Protein, g/g Cr	C_{cr}, ml/min
Normal adult human kidney (control)	12	2/10	55±6	0.70±0.04	14.8±1.2	0.06±0.02	100±11
Nephrectomy	7	2/5	68±5	0.79±0.04	16.9±1.3	0.04±0.01	95±23
Minor glomerular abnormalities	5	0/5	36±8	0.58±0.04	11.8±1.6	0.08±0.03	103±9
Human fetal kidney	10	5/5		ND	ND	ND	ND
IgAN	33	16/17	37±3	0.98±0.10*	15.6±1.4	0.86±0.16‡	84±5
MCNS	7	3/4	39±3	0.77±0.07	13.7±1.8	10.0±2.76‡	96±9
FSGS	9	6/3	57±2	1.23±0.14†	26.8±5.7	2.17±0.79‡	50±8*
MN	8	3/5	59±1	0.73±0.07	12.3±1.6	2.18±0.48‡	80±6
DN	29	22/7	59±2	1.35±0.12†	24.2±2.0*	6.14±0.96‡	55±9†

Values are means ± SE. *n*, No. of patients; sCr, serum creatinine; BUN, blood urea nitrogen; C_{cr}, creatinine clearance; IgAN, IgA nephropathy; MCNS, minimal change nephrotic syndrome; FSGS, focal segmental glomerulosclerosis; MN, membranous nephropathy; DN, diabetic nephropathy; ND, not determined. *$P < 0.05$, †$P < 0.005$, and ‡$P < 0.0005$ vs. control.

MATERIALS AND METHODS

Patients and tissue samples. Needle renal biopsy tissues were obtained from 86 patients treated at Kyoto University Hospital or Saiseikai Nakatsu Hospital with various glomerulopathies: 33 with IgA nephropathy (IgAN), 29 with type 2 diabetic nephropathy (DN), 7 with minimal change nephrotic syndrome (MCNS), 9 with focal segmental glomerulosclerosis (FSGS), and 8 with membranous nephropathy (MN). Diagnosis was confirmed by pathological evaluation of specimens, such as light microscopy, electron microscopy, and immunofluorescence staining. No patients received steroids or immunosuppressive drugs before biopsy. Ten human fetal kidneys (estimated gestational age ranging from 16 to 20 wk) were obtained fresh from tissues examined after therapeutic abortion at the Congenital Anomaly Research Center, Kyoto University Graduate School of Medicine. For normal controls, tissues obtained from seven patients afflicted with localized neoplasm using uninvolved portions of surgically removed kidneys and five biopsy samples from patients with minor glomerular abnormalities were used. Histopathological examination of control tissues excluded any glomerular diseases. This study was approved by the Ethics Committee of Kyoto University Graduate School of Medicine, and informed consent was obtained in accordance with protocols approved by the committee.

After resecting, the samples were fixed in Dubosq-Brazil solution. Table 1 summarizes details of the analyzed materials. Patients with IgAN were further classified as those with mild mesangial expansion (*group I*) and with severe mesangial expansion (*group II*), defined as a mesangial area <30% (*group I*) and >30% (*group II*) of total glomerular area, respectively. Clinical parameters of IgAN between two groups are summarized in Table 2.

Immunohistochemical analysis. Immunohistochemical analysis was performed as previously described with some modifications (32, 33). In brief, deparaffinized 3-μm kidney sections were treated with autoclave heating, and specimens were incubated with 1% Triton X-100 (Nacalai Tesque, Kyoto, Japan) in PBS for 20 min, washed three times with PBS, and incubated with 10% normal donkey serum in PBS for 10 min at room temperature. Goat antibody against the COOH terminus of human Cyr61 (CCN1; sc-8561, Santa Cruz Biotechnology, Santa Cruz, CA) or rabbit anti-human Wilms' tumor-1 (WT1) antibody (sc-192, Santa Cruz Biotechnology) was diluted 1:50 in PBS containing 1% BSA (1% BSA/PBS) and incubated for 1 h at room temperature. After blocking of endogenous phosphatase with 2 mM levamisole, the sections were incubated with alkaline phosphatase-conjugated donkey anti-goat or anti-rabbit IgG (Jackson ImmunoResearch, West Grove, PA) in 1% BSA/PBS for 30 min at room temperature. The sections were processed with NBT-BCIT (Roche Diagnostics, Mannheim, Germany) in alkaline buffer (100 mM Tris, pH 9.5, 100 mM NaCl, 50 mM $MgCl_2$) and counterstained with Kernechtrot stain solution (Muto Pure Chemicals, Tokyo, Japan). For double staining, the sections were pretreated with 3% hydrogen peroxide for 15 min at room temperature, incubated with peroxidase-conjugated secondary antibody against rabbit IgG (Jackson ImmunoResearch), and processed with 3,3′-diaminobenzidine tetrahydrochloride (Kanto Chemical, Tokyo, Japan). Nonimmune goat or rabbit serum was used as negative control.

Histological and morphometric analysis. Staining intensity of CCN1 and WT1 in kidney samples was examined by two independent investigators, and the score was averaged. At least six glomeruli per biopsy were evaluated at high-power magnification, and the intensity was semiquantified by a rating of 0–3 (most prominent). The number of CCN1- and WT1-positive cells per glomerular cross section was quantified as described elsewhere (33). Mesangial area was computer analyzed by measuring the periodic acid-Schiff (PAS)-positive area in cross sections of glomeruli scanned from vascular poles, using an automatic image analyzer (KS400, Carl Zeiss Vision, Munich, Germany) (35). To analyze CCN1 expression in cultured human podocytes, cells were fixed with 3.7% formaldehyde for 20 min followed by permeabilization with 0.1% Triton X-100 for 20 min at room temperature. After being rinsed with PBS, primary antibody anti-Cyr61 (CCN1; sc-8561, Santa Cruz Biotechnology) was applied for 60 min at room temperature. Antigen-antibody complexes were visualized using FITC-conjugated secondary antibody (705–095-147, Jackson ImmunoResearch). Confocal fluorescence microscopy was done with a laser-scanning microscope (Fluoview FV500, Olympus, Tokyo, Japan) with appropriate filters.

Purification of recombinant CCN. Conditioned media of Sf9 cells (Invitrogen, Carlsbad, CA) infected with baculovirus driving the

Table 2. *Clinical parameters of IgAN patients with mild (Group I) and severe (Group II) mesangial expansion*

	Gender (M/F)	Age, yr	sCr, mg/dl	BUN, mg/dl	Urinary Protein, g/g Cr	C_{cr}, ml/min	Mesangial Area (% of Total Glomerular Area)
Group I (*n* = 21)	11/10	30±2	0.85±0.06	13.5±1.2	0.58±0.13	96±4	26.0±1.2
Group II (*n* = 12)	5/7	42±5	1.28±0.20	19.1±3.2	1.42±0.31	62±9	37.1±1.5
P value, *group I* vs. *group II*		NS	NS	NS	$P < 0.05$	$P < 0.05$	$P < 0.0001$

Values are means ± SE. IgAN were classified into 2 groups defined as those with mesangial area <30% (*group I*) and >30% (*group II*) of total glomerular area, respectively. NS, not significantly different.

synthesis of CCN1 were used as a source for purification, as previously described (13). Full-length mouse CCN1 cDNA was generated by RT-PCR using total RNA from C57BL/6 mouse kidneys, and the following primers were used: sense, 5′-tgcgcgccacaatgagctccagca-3′ and antisense, 5′-ttagtccctgaacttgtggatgtc-3′ (nucleotides 179–1329, GenBank accession number M32490) (18). CCN1 cDNA was TA-cloned into pGEM-T Easy vector (Promega, Madison, WI) and transferred into pBacPAK vector (Clontech, Palo Alto, CA). The transfer vector along with BacPAK6 viral DNA (Clontech) was delivered into cells by liposome-mediated transfection to obtain a recombinant virus. Sf9 cells grown to 10^6 cells/ml in SFM-II medium were infected with the recombinant virus and incubated for 48 h at 28°C. The conditioned media centrifuged at 5,000 *g* for 5 min at 4°C were adjusted to 50 mM sodium phosphate buffer (pH 6.0) containing 2 mM EDTA and 1 mM PMSF and applied to a Hitrap SP column (Amersham, Piscataway, NJ) at 4°C. The column was washed with the same buffer containing 150 mM NaCl, and bound protein was subsequently eluted with a stepwise gradient of NaCl (0.2–1.0 M) in 50 mM sodium phosphate buffer (pH 6.0). The fractions were analyzed by 10% SDS-PAGE followed by Coomassie brilliant blue (Nacalai) staining or Western blotting. Fractions containing CCN1 were combined and adjusted to pH 7.5 with 0.5 M Tris·HCl/10% glycerol before storage in aliquots at −80°C. Protein concentration was determined by the modified Bradford method with a protein assay kit (Bio-Rad, Hercules, CA).

Cell culture. Human umbilical vein endothelial cells (HUVEC; Clonetics, Walkersville, MD) were maintained in the basal medium with growth supplements (EGM-2; Clonetics) containing 2% FCS (Cansera International, Ontario, Canada). Cell cultures between *passages 5* and *7* were used for each experiment. Mesangial cells established from glomeruli of 6-wk-old Sprague-Dawley rats were cultured in DMEM (Invitrogen) containing 10% FCS and antibiotics (32) and used between *passages 7* and *10*. Human mesangial cells (Clonetics) were maintained in the basal medium with growth supplements (CC-3147; Clonetics). Cell cultures between *passages 5* and *8* were used for each experiment.

Conditionally immortalized mouse podocytes (a kind gift from Dr. Peter Mundel) were cultured with RPMI 1640 medium (Nihonseiyaku, Tokyo, Japan) containing 10% FCS and antibiotics on dishes coated with type I collagen (Koken, Tokyo, Japan) as described elsewhere (24, 32). The cells proliferate when cultured at 33°C with 10 U/ml IFN-γ (Life Technologies, Gaithersburg, MD), whereas they halt growing and begin to differentiate when cultured at 37°C without IFN-γ. For CCN1 stimulation experiments, cells were differentiated for 2 wk and cultured with RPMI 1640/1% FCS for 24 h, until stimulation with recombinant CCN1 for 24 h on collagen I-coated dishes (Iwaki Glass, Chiba, Japan). Cells were used between *passages 15* and *20*. Conditionally immortalized human podocytes were cultured as described previously (33). These cells proliferate when cultured at 33°C, whereas they halt growing when cultured at 37°C. Cells were cultured

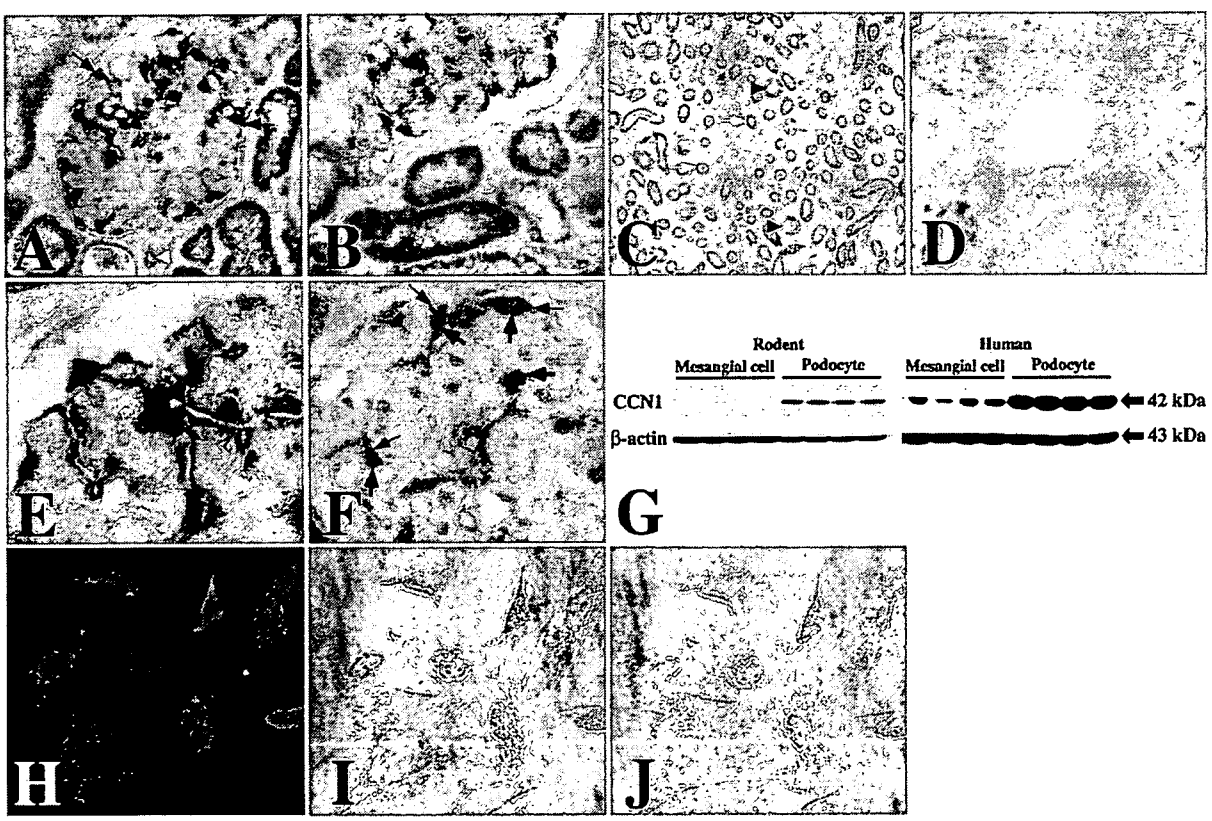

Fig. 1. Immunohistochemical analyses of cysteine-rich protein 61 (Cyr61; CCN1) expression in normal adult human kidney. CCN1 expression was detected at podocytes exclusively within the glomeruli (*A* and *F*, black arrows). CCN1-positive cells (*F*, black arrows) were also positive for WT1 (*F*, brown arrows). Weak CCN1 expression was also observed in some of arterioles (*A*, white arrowhead). Parietal epithelial cells, mesangial cells, and endothelial cells were negative for CCN1 in the glomeruli (*A*, *E*, and *F*). CCN1 expression was localized to the distal and proximal tubules (*B*), the thick ascending limb of Henle's loop (*C*, white arrows), and collecting ducts (*C*, black arrowheads). There was no detectable CCN1 expression within endothelial cells or smooth muscle cell of arteries (*D*). Cultured mouse and human podocytes significantly expressed a higher level of CCN1 compared with cultured rat and human mesangial cells, respectively (*G*). Confocal fluorescence microscopy revealed both cytoplasmic and nuclear expression of CCN1 (*H* and *J*, green) in human cultured podocytes (*I*, counterphase of *H*; *J*, merged image of *H* and *I*). Magnification: ×400 (*A*, *B*, *D*, *H–J*); ×200 (*C*); ×1,000 (*E* and *F*).

with RPMI 1640 medium (Sigma-Aldrich) supplemented with 10% FCS (Sigma-Aldrich) and an insulin-transferrin-sodium selenite media supplement (Sigma-Aldrich) on tissue culture dish (Corning, Corning, NY). Cells were differentiated at 37°C for 2 wk without passage and were subcultured on 96-well plates (146520, Nunc, Roskilde, Denmark). Cells were used between *passages 15* and *18*. For CCN1 expression analysis, cells grown at 33°C were used.

Northern and Western blot analyses. Northern blot analysis was performed as described elsewhere (32). In brief, after RNA extraction by TRIzol Reagent (Invitrogen), total RNA (20 μg in each lane) was electrophoresed on 1.0% agarose gels and transferred to nylon membranes (GeneScreen Plus, NEN, Boston, MA). The cDNA fragments of mouse synaptopodin (nucleotides 2165–2766, GenBank accession number XM_619543), mouse podocalyxin (nucleotides 1184–1601, GenBank accession number AF290209), mouse podoplanin (nucleotides 420–809, GenBank accession number BC026551), and mouse α-actinin-4 (nucleotides 2425–2809, GenBank accession number NM_021895) were generated by RT-PCR and used as probes. The membranes were hybridized with [^{32}P]dCTP-labeled probes, and the blots were exposed to a BAS-III imaging plate. The amount of RNA loaded in each lane was normalized for 28S ribosomal RNA.

Western blot analysis was performed as described elsewhere (16, 33). In brief, cells were lysed on ice in solution containing 20 mM Tris·HCl (pH 7.5), 12 mM glycerophosphate, 0.1 M EGTA, 1 mM pyrophosphate, 5 mM NaF, 5 mg/ml aprotinin, 2 mM dithiothreitol, 1 mM PMSF, 1% Triton X-100, and 1 mM sodium orthovanadate (Sigma-Aldrich). The lysate was centrifuged at 15,000 *g* for 20 min at 4°C, and the samples mixed with Laemmli's sample buffer were separated by 12.5% SDS-PAGE and transferred onto Immobilon filters (Millipore, Bedford, MA). The filters were incubated with rabbit anti-p27 (sc-528, Santa Cruz Biotechnology), goat anti-Cyr61 (CCN1; sc-8561, Santa Cruz Biotechnology), or mouse anti-β actin antibodies (A5441, Sigma-Aldrich) diluted in Block Ace (Snow Brand Milk Products, Sapporo, Japan) for 2 h at room temperature and were developed with horseradish peroxidase-conjugated donkey secondary antibodies (Santa Cruz Biotechnology) and a chemiluminescence kit (ECL plus, Amersham).

Cell adhesion assay. Adhesion of HUVEC and mesangial cells was analyzed using 96-well microtiter plates (Corning) coated with increasing concentrations of CCN1 protein diluted in PBS at 50 μl/well, followed by blocking with 1% BSA (14). For HUVEC, subconfluent cells were washed twice with PBS/1 mM EDTA/0.1% glucose and harvested by incubation in the same buffer for 15 min at room temperature. Cells were washed and resuspended in serum-free basal medium containing 0.2% BSA/10 mM HEPES (pH 7.2) at 4 × 10^6 cells/ml. The cell suspension was plated at 50 μl/well and allowed to adhere to protein-coated wells at 37°C for 20 min, followed by washing twice with PBS. Adherent cells were fixed with 10% formalin and stained with 1% methylene blue in 10 mM boric acid buffer (pH 8.5). Adhesion was quantified by measuring absorbance at 620 nm (14). For mesangial cells, subconfluent cells were washed twice with PBS and harvested by incubation in 0.1% trypsin/EDTA. Cells resuspended in DMEM/1.0% FCS at 10^6 cells/ml were plated at 50 μl/well and allowed to adhere to wells at 37°C for 50 min, followed by washing twice with PBS. Adherent cells were fixed and quantified as above.

Cell migration assay. Migration of mesangial cells and podocytes was analyzed by a modified Boyden chamber method using 96-well chambers (Neuro Probe, Gaithersburg, MD) as described elsewhere (4, 32). Polycarbonate filters (8 μm) coated with poly-L-lysine (Sigma-Aldrich) for mesangial cells, or type I collagen for podocytes, were placed in the middle of the chambers. Cells suspended in medium with 1% FCS (10^5 cells/well) were placed in the top chambers. CCN1 protein in medium with 1% FCS with or without PDGF-BB was added to the bottom chambers. After incubation for 3 h at 37°C, the cells that had migrated to the lower surface were fixed in methanol, stained with 0.5% Coomassie brilliant blue in 50% methanol/40% water/10% acetic acid, and quantified by measuring absorbance at 620 nm.

Statistical analysis. Results are given as means ± SE. A Mann-Whitney *U*-test was used to compare unpaired two-group means. Statistical analysis was performed with a Stat View (R) software package (Abacus, Berkeley, CA), and the difference with $P < 0.05$ was considered statistically significant.

RESULTS

CCN1 expression in normal adult human kidney. The immunohistochemical staining pattern of CCN1 in normal adult kidneys was essentially consistent in the 12 samples analyzed (Fig. 1, summarized in Table 3). Within the glomeruli, podocytes were invariably positive for CCN1 staining, whereas parietal epithelial cells, mesangial cells, and endothelial cells were virtually negative for CCN1 (Fig. 1*A*). Podocytes were identified morphologically as cells located at the outer aspect of the glomerular basement membrane (GBM) and immunohistochemically as WT1-positive cells (Fig. 1*F*). CCN1 expression in podocytes was detected mainly in the cytoplasm and also in the nucleus (Fig. 1, *A* and *E*). In tubular epithelial cells,

Table 3. *Summary of CCN1 expression in the adult kidney*

Cell Type	Normal	IgAN	MCNS	FSGS	MN	DN
Glomerulus						
Mesangial cells	−	−	−	−	−	−
Visceral epithelial cells (podocytes)						
Cytoplasm	+++	−~++	++~+++	++~+++	±~++	−~±
Nucleus	+++	−~++	++~+++	++~+++	±~++	+~+++
Parietal epithelial cells	−	−	−	−	−	−
Capillary endothelial cells	−	−	−	−	−	−
Vasculature						
Endothelial cells	−	−	−	−	−	−
Smooth muscle cells	−	−	−	−	−	−
Adventitial cells	−	−	−	−	−	−
Tubulointerstitium						
Proximal tubules	++	++	++	++	++	++
Distal tubules	++	++	++	++	++	++
Loop of Henle	+++	+++	+++	+++	+++	+++
Collecting ducts	++	++	++	++	++	++
Interstitial cells	−	−	−	−	−	−

CCN1, cysteine-rich protein 61.

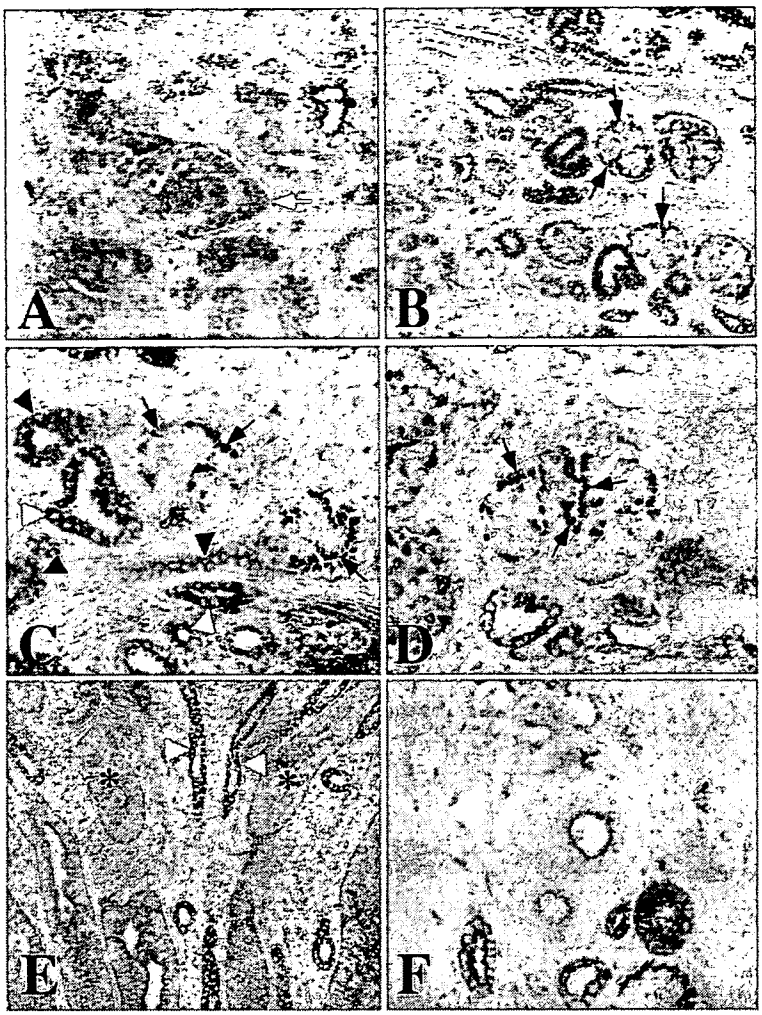

Fig. 2. Immunohistochemical analyses of CCN1 expression in fetal human kidney. CCN1 was negative or faintly positive in early glomerular stages (*A*, white arrow). From the late capillary loop stage, CCN1 expression was detected in developing podocytes (*B–D*, black arrows). There was also CCN1 expression in developing thick ascending limb of Henle's loop, distal tubules (*C* and *E*, white arrowheads), proximal tubules (*C*, black arrowheads), and collecting ducts (*E*, asterisks). CCN1 was also detected at endothelial cells in arteries and arterioles (*F*). Magnification: ×400 (*A*, *C*, and *F*); ×200 (*B* and *E*); ×1,000 (*D*).

CCN1 staining was positive in the thick ascending limb of Henle's loop, distal tubules, proximal tubules, and collecting ducts (Fig. 1, *B* and *C*). CCN1 expression in the tubular cells was prominent in the cytoplasm, and to a lesser extent in the nucleus (Fig. 1, *B* and *C*). Weak expression of CCN1 protein was also observed in some of afferent and efferent arterioles (Fig. 1*A*), but the protein was not expressed in larger vessels (Fig. 1*D*). Negative controls with nonimmune goat or rabbit serum gave no staining in all analyzed normal and diseased kidneys (data not shown). Compatible with human kidney tissue, cultured podocytes expressed abundant CCN1 compared with mesangial cells (Fig. 1*G*). Confocal fluorescence microscopy revealed both cytoplasmic and nuclear expression of CCN1 in human cultured podocytes (Fig. 1, *H–J*).

CCN1 expression in developing human kidney. In the developing human kidneys, CCN1 showed a distinct localization pattern (Fig. 2, summarized in Table 4). In early glomerular stages, i.e., comma-shaped and S-shaped bodies, CCN1 was almost completely negative in the glomeruli (Fig. 2, *A* and *B*). From the late capillary loop stage, CCN1 expression was detected in the glomeruli, restricted to the developing podocytes (Fig. 2, *B–D*). CCN1 expression in fetal podocytes was detected mainly in the nucleus and also in the cytoplasm (Fig. 2*D*). Intensity of CCN1 expression in podocytes was stronger in glomeruli at the maturing stage (Fig. 2, *B* and *C*). Other glomerular cell types, including developing endothelial cells, mesangial cells, and parietal epithelial cells, were uniformly

Table 4. *Expression of CCN1 in the fetal kidney*

Site	CCN1 Expression
Glomerulus	
Comma-shaped body	−
S-shaped body	−
Capillary loop stage	Visceral epithelial cells (podocytes) +~++
Maturing-stage glomeruli	Visceral epithelial cells (podocytes) ++~+++
Tubules	
Distal tubules	+++
Thick ascending limb of Henle	+++
Proximal tubules	++
Collecting ducts	+
Vasculature	
Arterial endothelial cells	+
Smooth muscle cells	−

negative for CCN1 (Fig. 2*D*). Strong CCN1 expression was detected in the developing thick ascending limb of Henle's loop, distal tubules, and proximal tubules (Fig. 2, *C* and *E*). Weak expression was present in developing collecting ducts (Fig. 2*E*). In the vasculature, CCN1 was detected at endothelial cells in arteries and arterioles (Fig. 2*F*).

CCN1 expression in IgAN. The CCN1 staining pattern was studied in 33 specimens with IgAN (Fig. 3, summarized in Tables 1–3). Cases included minimal lesions, those with mesangial hypercellularity and/or mesangial expansion, and those with severe focal necrosis and crescents (represented in Fig. 3, *F*, *H*, and *J*, respectively). In cases with IgAN, glomerular CCN1 expression was also confined to podocytes (Fig. 3, *C*, *E*, *G*, and *I*) as in normal glomeruli (Fig. 3*A*). WT1 staining in the nucleus as a podocyte marker in adjacent sections confirmed podocyte-specific expression of CCN1 (Fig. 3, *A–D*). In IgAN, however, the intensity of CCN1 staining in podocytes was decreased in various degrees compared with normal controls (Fig. 3*M*). Furthermore, some podocytes seemed to have lost CCN1 expression (Fig. 3, *C* and *E*). In contrast, WT1 staining intensity was not reduced in IgAN (Fig. 3*M*). Closer examination revealed that expression of CCN1 was markedly decreased in podocytes surrounding glomerular tufts with severe mesangial expansion (Fig. 3*G*) and in those adjacent to segmental sclerosis (Fig. 3*I*). Thus CCN1 staining intensity at podocytes was significantly reduced in cases with severe mesangial expansion (*group II*) compared with those with mild mesangial lesion (*group I*) (Fig. 3*N*, Table 2). The number of CCN1-positive cells per glomerulus was also significantly decreased in *group II* (Fig. 3*N*). Tubular CCN1 expression and its localization were well preserved in IgAN, even in tubular cells with advanced tubulointerstitial lesion (Fig. 3, *K* and *L*).

CCN1 expression in other glomerular diseases. Next, we evaluated cases with MCNS, FSGS, MN, and DN as glomer-

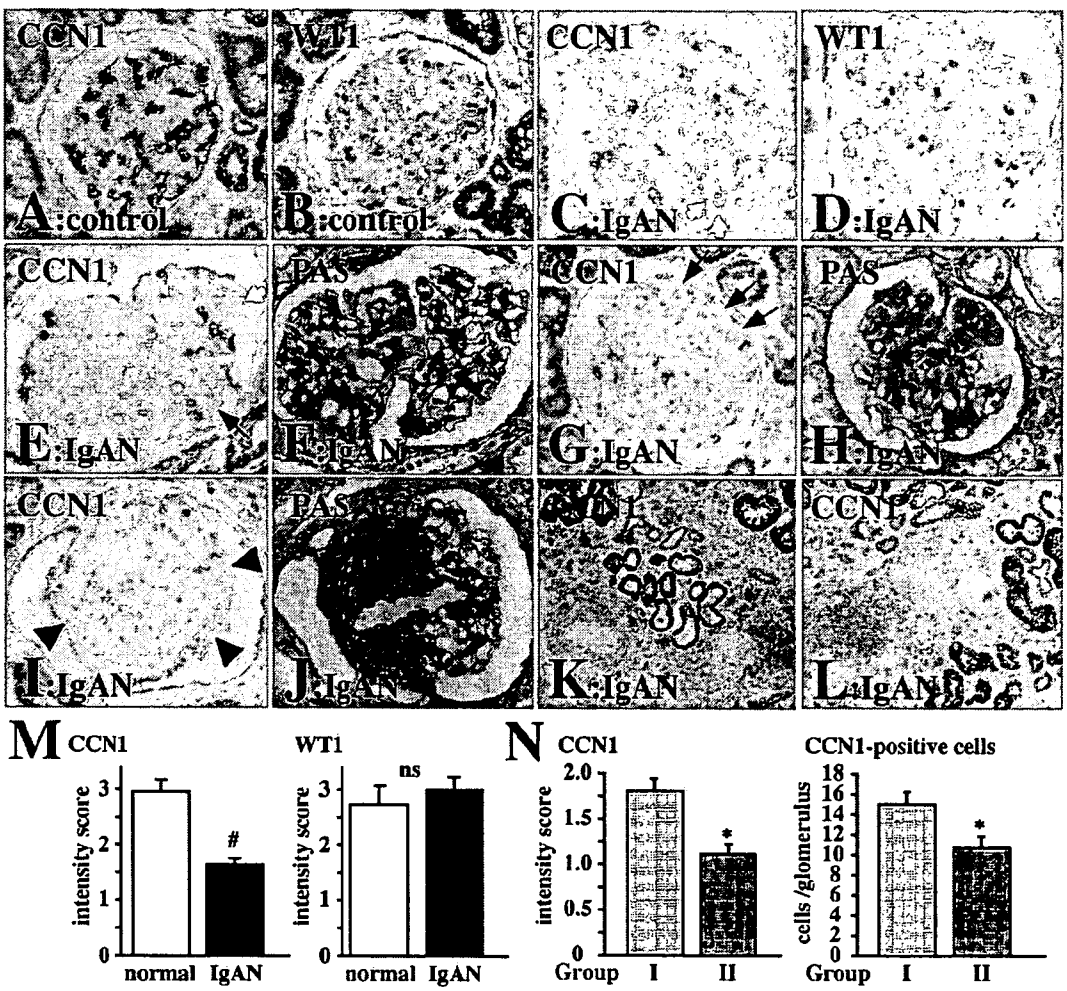

Fig. 3. CCN1 expression in IgA nephropathy (IgAN). CCN1 staining (*A*, *C*, *E*, *G*, *I*, *K*, *L*), WT1 staining (*B* and *D*), and periodic acid-Schiff (PAS) staining (*F*, *H*, and *J*) of renal biopsy specimens from patients with IgAN (*C–L*) and normal controls (*A* and *B*) is shown. Compared with normal controls (*A*), CCN1 staining intensity at podocytes was decreased in IgAN (*C*, *E*, *G*, and *I*). Expression of CCN1 was downregulated especially in podocytes surrounding the glomerular tuft with mesangial expansion (*G*, black arrows), and in podocytes next to segmental sclerosis (*I*, black arrowheads). CCN1-negative podocytes were frequently observed (white arrows). CCN1 expression was well preserved in the tubular cells (*K* and *L*). Intensity of CCN1 expression in podocytes was significantly decreased in IgAN compared with normal controls, whereas intensity of Wilms' tumor-1 (WT1) was not altered (*M*). Decrease in CCN1 intensity and the number of CCN1-positive cells was prominent in IgAN with severe mesangial expansion (*group II*) compared with those with only mild mesangial expansion (*group I*; *N*). ns, Not significantly different. Magnification: ×400 (*A–J*); ×200 (*K* and *L*). #$P < 0.005$ vs. normal control. *$P < 0.005$ vs. *group I*.

ular disease with various degrees of mesangial expansion (Fig. 4, summarized in Table 3). CCN1 expression was also confined to podocytes in these glomerulopathies (Fig. 4, *C*, *E*, *G*, and *I*). In cases with MCNS or FSGS, the intensity of CCN1 expression in podocytes was decreased in some glomeruli, but not with statistical significance (Fig. 4, *C*, *E*, and *K*). Podocyte CCN1 expression was significantly decreased in cases with MN (Fig. 4, *G* and *K*), and also in DN, which had a prominent decrease in cytoplasmic CCN1 (Fig. 4, *I* and *K*, Table 3). CCN1-positive cells per glomerular cross section were decreased in all of the glomerular diseases examined, which in part may be due to a loss of podocytes, indicated by decreased WT1-positive cells per glomerular cross section (Fig. 4*L*). However, the ratio of CCN1-positive cells to WT1-positive cells was significantly decreased in IgAN by 23% but was not altered in MCNS, FSGS, MN, and DN (Fig. 4*L*). CCN1-negative podocytes frequently seen in IgAN were not observed in these glomerular diseases. WT1 staining intensity was not altered in any of these diseases (Fig. 4, *D*, *F*, *H*, *J*, and K). Tubular CCN1 was preserved in MCNS, FSGS, MN, and DN (data not shown), as was the case with IgAN (Fig. 3, *K* and *L*).

Effects of CCN1 on mesangial cell adhesion and migration. To clarify the functional role of CCN1 expressed at podocytes, effects of recombinant CCN1 protein were examined in vitro. Because CCN1 expression at podocytes was decreased in glomeruli with mesangial expansion, we examined the effects of CCN1 on mesangial adhesion and migration. Although CCN1 significantly augmented endothelial cell attachment (Fig. 5*A*) as in previous reports (13, 14), CCN1 caused a marked inhibition of mesangial cell adhesion (Fig. 5*A*). Next, we examined the effect of CCN1 on mesangial migration. In the presence of PDGF-BB, CCN1 potently abolished PDGF-induced mesangial migration (Fig. 5*B*). These results show that CCN1 can act on mesangial cells as a potential inhibitor of adhesion and migration.

Effects of CCN1 on podocyte differentiation. To explore the role of CCN1 on podocytes, podocytes cultured under differ-

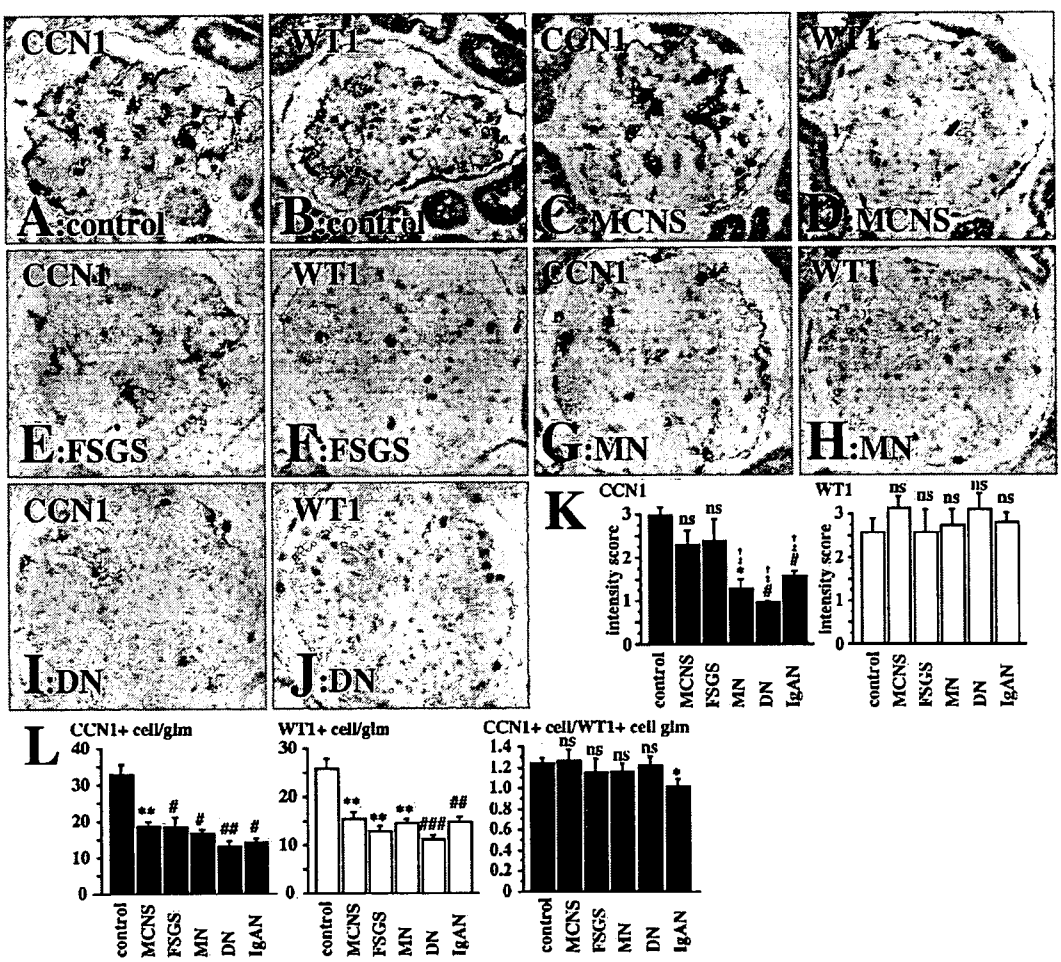

Fig. 4. CCN1 expression in minimal change nephrotic syndrome (MCNS), focal segmental glomerulosclerosis (FSGS), membranous nephropathy (MN), and diabetic nephropathy (DN). CCN1 staining (*A*, *C*, *E*, *G*, and *I*) and WT1 staining (*B*, *D*, *F*, *H*, and *J*) of normal controls (*A* and *B*), MCNS (*C* and *D*), FSGS (*E* and *F*), MN (*G* and *H*), and DN (*I* and *J*) is shown. CCN1 expression in podocyte cytoplasm was significantly decreased in MN and DN compared with normal controls, MCNS, and FSGS (*A*, *C*, *E*, *G*, *I*, and *K*), whereas the intensity of WT1 in podocytes was not altered (*B*, *D*, *F*, *H*, *J*, and *K*). CCN1-positive cells as well as WT1-positive cells per glomerular cross section (glm) were decreased in all of the glomerular diseases examined, and the ratio of CCN1-positive cells to WT1-positive cells was significantly decreased in IgAN (*L*). Magnification: ×400 (*A*–*J*). $*P < 0.05$ vs. normal control. $**P < 0.01$ vs. normal control. $\#P < 0.005$ vs. normal control. $\#\#P < 0.001$ vs. normal control. $\#\#\#P < 0.0005$ vs. normal control. $\dagger P < 0.05$ vs. MCNS. $\ddagger P < 0.05$ vs. FSGS.

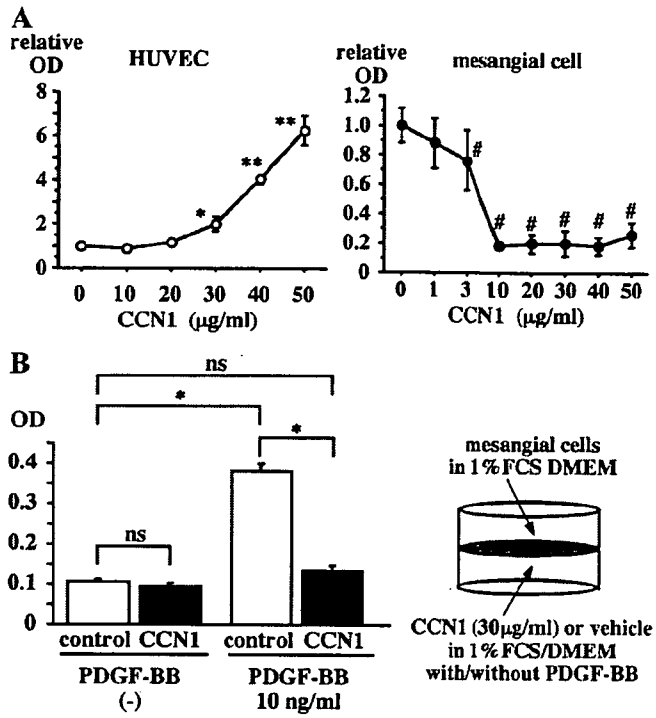

Fig. 5. Effects of CCN1 on mesangial cell adhesion and migration. Purified CCN1 protein enhanced adhesion of human umbilical vein endothelial cells (HUVEC) but potently inhibited mesangial cell adhesion (*A*). Recombinant CCN1 showed almost complete inhibition of PDGF-induced migration at 30 μg/ml (*B*). $*P < 0.05$, $**P < 0.005$, and $\#P < 0.01$ vs. control; $n = 5$–6.

entiating condition for 2 wk were incubated with recombinant CCN1 for an additional 24 h. Synaptopodin, a marker widely used to identify differentiated phenotypes of podocytes, was upregulated dose dependently (Fig. 6, *A* and *C*). Other podocyte-specific genes including podocalyxin, podoplanin, and α-actinin-4, were not significantly induced by addition of CCN1. Since differentiation of podocytes leads to a quiescent phenotype both in vitro and in vivo (5, 25, 34), we examined the effect of CCN1 on $p27^{Kip1}$ (p27) expression, a cyclin-dependent kinase inhibitor (CKI) involved in the maintenance of G0/G1 phase arrest in podocytes (5). CCN1 upregulated p27 protein dose dependently (4.2-fold with 3 μg/ml CCN1) (Fig. 6, *B* and *C*). Because the migratory phenotype of podocytes is reported to be involved in glomerulosclerosis (17, 30, 31), we finally examined the effect of CCN1 on podocyte migration. CCN1 significantly suppressed podocyte migration by 26% (Fig. 6*D*). Thus CCN1 may act as an autocrine/paracrine factor, promoting podocyte differentiation and maintaining its quiescent phenotype.

DISCUSSION

In the present study, we investigated CCN1 protein expression in normal fetal and adult human kidneys and those with various nephropathies. In normal glomeruli, CCN1 was predominantly expressed at podocytes from the capillary loop stage to mature glomeruli. CCN1 was also present in the thick ascending limb of Henle's loop, distal and proximal tubules, and collecting ducts. Decrease in CCN1 expression at podocytes was observed in IgAN, DN, and MN. Especially in IgAN, CCN1-negative podocytes were frequently observed, and the intensity of CCN1 staining at podocytes was significantly reduced in cases with severe mesangial expansion. In vitro, CCN1 prominently inhibited adhesion and migration of mesangial cells. Furthermore, CCN1 induced p27 and synaptopodin expression, indicating that CCN1 may act as an autocrine factor to stimulate podocyte differentiation.

CCN1 at podocytes may exert its function in two ways: one in a secreted form, and the other as a factor inside the nucleus. Secreted CCN1, which may be quantified by CCN1 staining at the cytoplasm, can act on glomerular cells in a GBM-bound form, since CCN1 has a high affinity for heparan sulfate proteoglycans (37), a major component of the GBM (8). Furthermore, CCN1 interacts with a variety of integrins (3, 9, 14, 19, 28), e.g., acting through integrin $\alpha_v\beta_3$ on endothelial cells and through $\alpha_v\beta_5$ on fibroblasts (9, 14), both of which are expressed in mesangial cells and podocytes (10). It was recently reported that production of vascular endothelial growth factor A, a homodimeric glycoprotein of 48 kDa, from podocytes is required for mesangial cell survival in vivo (6), suggesting that secreted factors from podocytes can act on glomerular cells, counteracting against the flow from the capillary lumen to the urinary space. It is therefore likely that CCN1, an extracellular matrix-associated protein with a similar molecular weight, secreted from podocytes can either act on

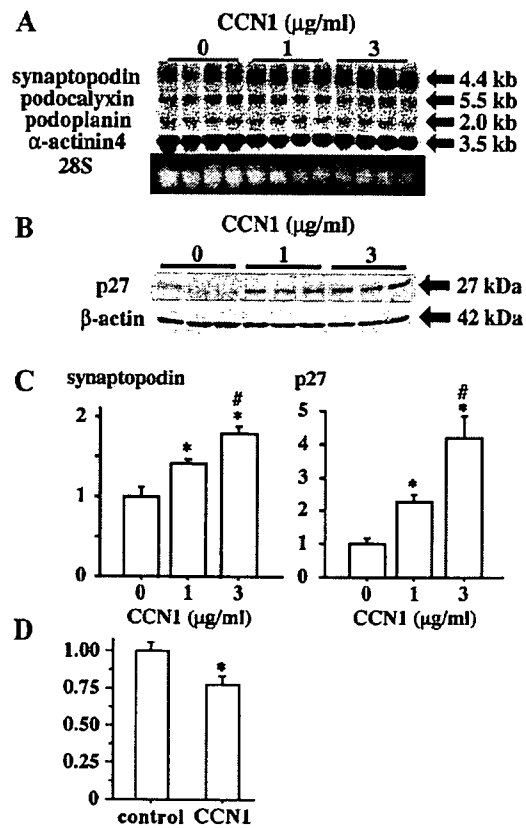

Fig. 6. Effects of CCN1 on cultured podocytes. Recombinant CCN1 enhanced the expression of synaptopodin mRNA (*A*) and cyclin-dependent kinase inhibitor p27 protein (*B*) in a dose-dependent manner (*C*). Podocyte migration was significantly suppressed by addition of CCN1 at 3 μg/ml (*D*). $*P < 0.05$ vs. 0 μg/ml. $\#P < 0.05$ vs. 1 μg/ml; $n = 4$.